Dynamic Transcriptome, Accessible Genome and PGR Cistrome Profiles in the Human Myometrium

San-Pin Wu[1], Matthew L. Anderson[2], Tianyuan Wang[3], Lecong Zhou[3], Olivia M. Emery[1], Xilong Li[4], and Francesco J. DeMayo[1]

[1]Reproductive & Developmental Biology Laboratory, [3]Integrative Bioinformatics Support Group, National Institute of Environmental Health Sciences, Research Triangle Park, NC 27709. [2]Department of Obstetrics & Gynecology, University of South Florida Morsani College of Medicine and Moffitt Cancer Center, Tampa, FL. [4]Department of Molecular and Cellular Biology, Baylor College of Medicine, Houston, TX77030.

Corresponding:

Francesco J. DeMayo, Ph.D.

Reproductive and Developmental Biology Laboratory

National Institute of Environmental Health Sciences

National Institutes of Health

111 T. W. Alexander Dr.

Research Triangle Park, NC 27709

TEL: +1 (984) 287-3987

E-mail: francesco.demayo@nih.gov

Keywords:, Human myometrial tissue, Transcriptome, PGR Cistrome, Genome accessibility.

Abstract

The myometrium undergoes structural and functional remodeling during pregnancy. We hypothesize that myometrial genomic elements alter correspondingly in preparation for parturition. Human myometrial tissues from nonpregnant (NP) and term pregnant (TP) human subjects were examined by RNAseq, ATAC-seq and PGR ChIP-seq assays to profile transcriptome, assessible genome and PGR occupancy. NP and TP specimens exhibit 2890 differentially expressed genes, reflecting an increase of metabolic, inflammatory and PDGF signaling, among others, in adaptation to pregnancy. At the epigenome level, patterns of accessible genome change between NP and TP myometrium, leading to altered enrichment of binding motifs for hormone and muscle regulators such as the progesterone receptor (PGR), Krüppel-like factors and MEF2A transcription factors. PGR genome occupancy exhibits a significant difference between the two stages of the myometrium, concomitant with distinct transcriptomic profiles including genes such as *ENO1*, *LHDA*, and *PLCL1* in the glycolytic and calcium signaling pathways. Over-representation of SRF, MYOD and STAT binding motifs in PGR occupying sites further suggests interactions between PGR and major muscle regulators for myometrial gene expression. In conclusion, changes in accessible genome and PGR occupancy are part of the myometrial remodeling process and may serve as mechanisms to formulate the state-specific transcriptome profiles.

42 **Introduction**

43 Myometrium is the muscular component of the uterus consisting of primarily smooth muscle and
44 vascular cells. The main function of the myometrium is to maintain structural integrity of uteri
45 during pregnancy and to provide contraction force for parturition. Myometrial smooth muscle
46 cells increase in number and size as well as change from a synthetic to a contractile state during
47 gestation [1, 2]. These cells need to remain quiescence before parturition and produce phasic
48 contractions at the laboring stage [3]. After parturition, the involution process reduces the size of
49 uterus to the nonpregnant state [4, 5]. Disorders associated with the myometrium may result in
50 preterm birth, dystocia, adenomyosis and leiomyoma, which impose serious burdens on maternal
51 and child health.

52 Steroid hormones progesterone, estrogen and glucocorticoid have been indicated for regulating
53 gene expression and cell proliferation of myometrial smooth muscle [6-10]. Estrogen modulates
54 contraction-associated genes and induces hyperplasia of myometrial smooth muscle cells at early
55 gestation by activating the PI3K/mTOR pathway and repressing myostatin expression [7, 8, 11,
56 12]. Estrogen also supports the expansion of myometrial progenitor-like cells [13] and works
57 together with progesterone to promote proliferation of leiomyoma side-population cells through
58 regulation of the paracrine WNT signaling from the mature myometrial cells. [14]. On the other
59 hand, progesterone signaling downregulates expression of genes that are associated with cell
60 proliferation in cultured human myometrial cells and has a negative effect on vascular smooth
61 muscle proliferation [9, 15, 16]. In contrast, glucocorticoids inhibits proliferation of uterine
62 leiomyoma cells, vascular smooth muscle cells and airway smooth muscle cells but has no
63 impact on the cell cycle progression in cultured uterine smooth muscle cells[6, 17, 18]. The role
64 of progesterone and glucocorticoid in the early gestation myometrium remains unknown.

65 Progesterone is also an FDA-approved tocolytic agent to prevent premature parturition [19].
66 Progesterone signaling is primarily mediated by the progesterone receptor (PGR) and is sensitive
67 to environmental endocrine disruptor [16, 20]. Mechanisms that control progesterone signaling
68 include metabolism of progesterone, transcription regulation and post translational modifications
69 of PGR and interaction between PGR and coregulators [21-25]. Before parturition, myometrial
70 progesterone signaling suppresses inflammatory and contractile activities via the ZEB1/ZEB2-
71 miR-200-STAT5b pathway, the PGR-AP-1 containing transcription repressive complex and

72 cAMP-DUSP1 dependent regulation of PGR phosphorylation [23, 26, 27]. At the transition to
73 the laboring stage, emerging reports suggest that the elevated ratio of PGR isoform A verse B
74 could turn the effect of progesterone signaling from repressive to inductive on transcription of
75 labor genes such as GJA1 and further promotes gap junction coupling in the myometrium [27-
76 29]. These findings demonstrate the versatility of the progesterone signaling in the myometrial
77 biology manifested by the activity of its cognate receptor PGR.

78 This study focuses on the physiological change between nonpregnant and term pregnant
79 myometrium. The profiles of transcriptome, open chromatin regions and PGR cistrome in human
80 myometrial specimens at both stages are documented to identify genetic pathways and potential
81 underlying mechanisms that may be responsible for the structural and functional adaptation to
82 pregnancy. The common and distinct molecular features of myometrium at these two stages not
83 only provide clinical relevance to known pathways but also suggest novel mechanisms that may
84 contribute to myometrial remodeling in support of pregnancy.

85

86 **Materials and Methods**

87 *Human Myometrial Specimens*

88 Permission to work with human tissue specimens for all experiments was obtained from
89 the Institutional Review Board for Baylor College of Medicine (BCM H-22119, Approved
90 5/7/2008). All specimens were obtained from the Gynecologic Tissue Repository for BCM,
91 which has previously been granted permission to routinely collect specimens of female
92 reproductive tract tissues under a separate IRB protocol (H-33461). Written informed consent is
93 available for all specimens utilized to perform the work described.

94 For the purposes of these experiments, specimens of myometrium were collected from
95 non-laboring gravid women at term (TP; 38-42 weeks estimated gestational age) undergoing
96 cesarean section for routine clinical indications. All myometrial specimens from gravid women
97 were collected from the margins of the hysterotomy following delivery of the fetus. No
98 specimens were collected from women who had undergone pitocin-induced augmentation of
99 labor within 6 hours of surgery or who had previously received 17-hydroxyprogesterone for the
100 treatment of pre-term labor. In addition, no specimens were collected from women whose

101 pregnancy had been complicated by other medical conditions (including but not limited to
102 gestational diabetes >IB, chorioamnionitis, pregnancy-induced hypertension, preeclampsia,
103 HELLP syndrome or its variants). Specimens of non-gravid myometrium (NP) were obtained
104 from healthy, pre-menopausal women undergoing routine, clinically-indicated gynecologic
105 surgery. All non-gravid myometrial specimens were collected from healthy myometrium at sites
106 that excluded both the uterine serosa and endometrium and were at least 2 cm from the nearest
107 leiomyoma. Any specimens from women using progestins prior to their surgery were excluded
108 from analysis.

109 After washing each specimen briefly in phosphate buffered saline (PBS), pieces of myometrium
110 were either flash frozen (ChIP-Seq) or preserved by plunging them into ice-cold RNALater
111 (RNA-Seq) with warm ischemia time less than 30 minutes. All specimens weresubsequently
112 stored at <-80°C until use. Assays for each individual sample are listed in Table S1.

113 *RNA Extraction*

114 Myometrial specimens were homogenized by the bead Mill 24 homogenizer (15-340-163, Fisher
115 Scientific, Waltham, MA) in Bead Mill Tubes (15-340-154 Fisher Scientific, Waltham, MA)
116 with 1 mL Trizol (15596026, Thermo Fisher Scientific, Waltham, MA). Tissue debris was
117 pelleted and removed by centrifugation at 12000 xg for 10 minutes at 4°C. After adding 200 uL
118 1-Bromo-3-chloropropane, samples were manually shake for 20 seconds followed by incubation
119 at room temperature for 3 minutes. Phase separation was conducted by centrifugation at 12000
120 xg for 18 minutes at 4°C. The RNA containing aqueous layer was retained and subsequently
121 mixed with 500 uL 200 proof ethanol. The mixture was then passed through the RNA binding
122 column of RNeasy Mini Kit (74104, Qiagen, Germantown, MD), followed by washing and
123 elution steps described in the manufacture's handbook.

124 *RNAseq*

125 The libraries prepared from myometrial specimens were sequenced with approximately 50
126 million, 101bp paired-end reads per sample. The raw reads were subsequently processed by
127 filtering with average quality scores greater than 20. Then the reads were aligned to hg19 using
128 TopHat version 2.0.4 [30]. Expression values of RNA-seq were expressed as FPKM (fragments
129 per kilobase of exon per million fragments) values. Differential expression was calculated using

130 Cufflink version 2.2.1 [31]. Functional analysis of gene lists was performed using the Ingenuity
131 Pathway Analysis (IPA, www.ingenuity.com) and The Database for Annotation, Visualization
132 and Integrated Discovery (DAVID) v6.8 [32, 33].

133 *ATACseq*

134 Three nonpregnant (NP) and 3 term pregnant (TP) myometrial specimens were sent to Active
135 Motif (Carlsbad, CA) for the library preparation service (catalog number 25079). The libraries
136 were generated with the Illumina Nextera DNA Library Prep kit and were sequenced by Active
137 Motif and NIEHS Sequencing core by Illumina HiSeq 2000 and NextSeq 500 systems with 42bp
138 paired-end reads on each sample. The raw reads were initially processed by trimming adaptors
139 and filtering with average quality scores greater than 20. The reads passing the initial processing
140 were aligned to the human reference genome (hg19) using bowtie version 1.1.2 [34]. After
141 removing the reads mapped to mitochondria DNA, the uniquely mapped deduplicated reads in
142 each sample were normalized by down-sampling to 91.5M single reads. Only the first 9bp of
143 each read were used for downstream analyses. The open chromatin regions (OCRs) were first
144 identified by MACS2 [35] with a cutoff of adjusted p-value 0.0001, followed by merging
145 genomic intervals within 100bp of each other.

146 Motif analysis and peak annotation to nearby gene within 25Kb were performed by the
147 Hypergeometric Optimization of Motif EnRichment (HOMER) motif discovery tool [36]. The
148 bivariate genomic footprinting (BaGFoot) algorithm [37] was used to identify binding motifs
149 exhibiting change of chromatin accessibility including footprint depth and flanking accessibility
150 between 2 myometrial stages.

151 *ChIPseq*

152 Chromatin immunoprecipitation and library preparation and sequencing were performed by
153 Active Motif (catalog number 25006 and 25046, Carlsbad, CA) using an anti-PGR antibody (sc-
154 7208, Santa Cruz Biotechnology, Dallas, TX) and a custom Illumina library with the standard
155 Illumina PE adaptors [38]. The Illumina HiSeq 2000 system was utilized for next generation
156 sequencing. The 50-nt single-end sequence reads identified were mapped to genome assembly
157 hg19 using the BWA algorithm with default settings. Only reads that passed Illumina's purity
158 filter and of a mean quality score of 20 or higher, aligned with no more than 2 mismatches, and

159 mapped uniquely to the genome were used in the subsequent analysis. In addition, unless stated
160 otherwise, duplicate reads were removed using the MarkDuplicates tool available in picard-tools-
161 1.119. The retained read alignments were sorted by coordinates, extended to 300 bases, and then
162 randomly downsampled to 9 million intervals per sample with custom scripts. MACS (version
163 2.1.1.20160309) was employed to perform peak calling with FDR cutoff at 0.0001, using a
164 human myometrium input as control. HOMER's "annotatePeaks.pl" and findMotifsGenome.pl"
165 functions with default settings were used for peak annotation and motif enrichment analysis of
166 given peak ranges [36]. BEDTools version 2.27.1 was chosen for merging and intersecting peaks
167 in overlapping analysis, with the default settings [39].

168 *ChIP-qPCR*

169 ChIP-qPCR was performed by Active Motif (Carlsbad, CA) using an anti-PGR antibody (sc-
170 7208, Santa Cruz Biotechnology, Dallas, TX). Primer sequences for the ChIP-qPCR assay are
171 ENO1_cF: AGCCCTTCCCCAATCATTAC, ENO1_cR: TACGTTCACCTCGGTGTCTG,
172 LDHA_cF: GTGCATTCCCGGTACGGTAG, LDHA_cR: AGCAGAACCAGAGGCAGTTG,
173 PLCL1_cF: GGAGAATGCGGGTCATCTTG, PLCL1_cR:
174 CAGGAAACAAGCAGGAGTAGG and Untr12 (Catalog #71001, Active Motif, Carlsbad, CA).
175 PGR binding events were calculated according to an equation published in the user's manual of
176 Active Motif catalog number 12970399.

177 *Quantitative RT-PCR*

178 cDNA was generated by the Transcriptor First Strand cDNA Synthesis Kit (04379012001,
179 Roche Life Science, Penzberg, Germany) in accordance to the manufacture's manual. PCR was
180 conducted by using SsoAdvanced Universal SYBR Green Supermix (1725270, Bio-Rad,
181 Hercules, CA) or SsoAdvanced Universal Probes Supermix (1725280, Bio-Rad, Hercules, CA)
182 on the CFX Connect Real-Time PCR Detection System (1855201, Bio-Rad, Hercules, CA)
183 based on manufacture's instruction.

184 Primers used in this study include OXTR_F: GGGGAGTCAACTTTAGGTTCG, OXTR_R:
185 TTCCTCGGGATGTTCAGC, GJA1_F: GCCTGAACTTGCCTTTTCAT, GJA1_R:
186 CTCCAGTCACCCATGTTGC, ZEB1_F: CCTAAAAGAGCACTTAAGAATTCACAG,
187 ZEB1_R: CATTTCTTACTGCTTATGTGTGAGC, PLCL1_F:

188 CAGGAAAAGATTGTACAGTGTCAGA, PLCL1_R: TTTGCCCCCAAATTATGAAG,
189 SLC2A1_F: GGTTGTGCCATACTCATGACC, SLC2A1_R:
190 CAGATAGGACATCCAGGGTAGC, HK2_F: GCTGAAGGAAGCGATCCA, HK2_R:
191 GTGTCGTTCACCACAGCAAC, ALDOB_F: GGCAAGGCTGCAAACAAG, ALDOB_R:
192 CCCGTGTGAACATACTGTCCT, PGK1_F: CAGCTGCTGGGTCTGTCAT, PGK1_R:
193 GCTGGCTCGGCTTTAACC, ENO1_F: TCCCAACATCCTGGAGAATAA, ENO1_R:
194 ATGCCGATGACCACCTTATC, PKM2_F: ACGTGGATGATGGGCTTATT, PKM2_R:
195 CCAAGGAGCCACCATTTTC, LDHA_F: GTCCTTGGGGAACATGGAG and LDHA_R:
196 TTCAGAGAGACACCAGCAACA. The 18S rRNA probe is from ThermoFisher Scientific
197 (4319413E, ThermoFisher Scientific, Waltham, MA). All the RT-PCR results were normalized
198 to the expression levels of the internal control 18S rRNA.

199 *High Content Data Deposit*

200 The RNAseq, ChIPseq and ATACseq raw data is under the SuperSeries GSE137552 in the Gene
201 Expression Omnibus of the National Center for Biotechnology Information at the National
202 Library of Medicine.

203

204 **Result**

205 <u>Adaptive Myometrial Transcriptome for Pregnancy</u>

206 Previous studies show that the expression of parturition associated genes *OXTR* and *GJA1*
207 increase and *ZEB1* and *PLCL1* decrease expression at the transition from quiescence to labor in
208 the term pregnant myometrium [40-43]. After examining 6 nonpregnant (NP) and 9 term
209 pregnant (TP) myometrial specimens, we extend these findings by demonstrating that mRNA
210 levels of *OXTR, GJA1, ZEB1* and *PLCL1* genes all start lower in the nonpregnant myometrium
211 and rise toward term pregnancy (Figure 1). These observations suggest that the myometrial
212 transcriptome is dynamically staged over the course of pregnancy in preparation for parturition.

213 Genome-wide transcriptome dynamics from the NP to the TP stage was further investigated by
214 RNAseq in a cohort of myometrial specimen independent from those in the aforementioned
215 study of marker genes (Table S1). Using a criteria of average fragments per kilobase of transcript

216 per million mapped reads (FPKM) greater or equal than 1 in at least one of the six specimens,
217 15907 active genes were found in the myometrium (Table S2). Within each group, the NP and
218 TP myometrium each has 14899 and 15260 active genes, respectively (Table 1 and Table S2).
219 Between these two stages, NP and TP samples share 14612 active genes (Table S2). While
220 95.7% NP and 93.4% TP expressing genes are present in both stages (Table 1), overall
221 transcriptome profiles exhibited a significant difference as evidenced by the principle component
222 analysis that shows distinct separation between samples of TP and NP stages (Figure 2A). These
223 findings suggest that the pregnancy dependent transcriptome dynamics in the myometrium is
224 primarily a result of change of mRNA levels rather than the composition of expressing genes.

225 Using the absolute fold change greater or equal to 1.4 and adjusted *p*-value less than 0.05 as the
226 cutoff, 2890 differentially expressed genes (DEGs) were identified between the two stages of
227 myometrium with expression of 1043 and 1847 genes relatively higher in NP and TP tissues,
228 respectively (Figure 2B). Parturition related genes again show increased expression toward term
229 pregnancy in this cohort of specimens with mean fold changes at 156 for *OXTR*, 2.9 for *GJA1*,
230 1.6 for *ZEB1* and 2.6 for *PLCL1* (Table S2), consistent with previous observations in another
231 cohort of specimens (Figure 1). Gene ontology analysis on the DEGs shows that genes expressed
232 at higher levels at the NP stage are enriched in terms in association with transcription, RNA-
233 binding and histone deacetylase activity among others, reflecting the synthetic state of the NP
234 myometrium. In contrast, terms linked to innate immunity, protease and carbohydrate transport
235 and metabolism are over-represented among genes of higher expression levels at pregnancy
236 (Tables 2 and S3), demonstrating a molecular profile of the contractile state in favor of
237 inflammation control, extracellular remodeling and increased energy demand as well as in
238 preparation for subsequent parturition. Further examining the 2890 DEGs reveals potential
239 alterations of molecular activities between NP and TP stages, as predicted by the differential
240 expression of downstream target genes of molecules of interest. The Ingenuity Pathway Analysis
241 (IPA) estimates increased activities of myometrial expansion/remodeling associated TGFβ,
242 PDGF, ERK and STAT, inflammation management linked TNF and AP-1, as well as myometrial
243 contraction related p53 signaling, among others (Table 3 and Table S4) [11, 44-49]. Changes of
244 these molecular activities appear to be evolutionarily conserved, as evidenced by a similar
245 observation that compares transcriptomic profiles of the mouse myometrium between 18.5 days
246 post coitus and virgin (GSE17021, Table 3 and Table S5). Notably, majority of the subset of

247 DEGs that match IPA curated glucose downstream exhibits changes of gene expression
248 consistent with the response to glucose treatment (Table 3, Table S4 and Table S5), which
249 suggests relatively higher glucose utilization at the TP stage. This result is also in line with the
250 aforementioned gene ontology enrichment finding as shown in Table 2. Moreover, genes that
251 encode enzymes of the glycolysis pathway, including *SLC2A1, ALDOB, PGK1, ENO1, PKM2*
252 and *LDHA*, exhibited increased mRNA levels toward term pregnancy in two independent cohorts
253 of specimens (Figure 3 and Table S2). The HK2 gene, which encodes the hexokinase for glucose
254 phosphorylation, also showed significant higher expression levels in the TP myometrium in the
255 first cohort despite displayed a trend of increase in the second cohort instead (Figure 3). The
256 higher expression in glycolytic pathway genes and glucose downstream targets together suggest
257 an increase of glucose usage in the TP myometrium compared with that in the NP stage. Taking
258 together, these findings illustrate an adaptive myometrial transcriptome in response to the
259 pregnancy and in preparation for parturition at various aspects such as structure reorganization,
260 inflammation and contraction management, and metabolic adaptation.

261

262 Accessible Genome Dynamics in the Myometrium

263 Since the myometrial transcription profiles are adaptive to pregnancy, we next examine the
264 myometrial genome accessibility to check if the profiles of open chromatin regions are also
265 different between NP and TP states. The assay for transposase-accessible chromatin using
266 sequencing (ATAC-seq) [50] was performed on myometrial specimens of three human subjects
267 of each stages. The NP and TP myometrium each has 45501 and 85777 open chromatin regions
268 (OCRs) identified in at least one of three samples within the group (Figure 4 and Table S6).
269 Among these genomic regions, 9564 (class I) and 50840 (class III) OCRs are exclusively present
270 in the NP and TP states, respectively, whereas 35937 OCRs (class II) can be detected in both
271 states (Figure 4). Within each class of OCRs, HOMER identified enrichment of 128, 82 and 121
272 transcription factor binding motifs in class I, II and III OCRs, respectively (Table S7). Among
273 these enriched motifs, 38, 2 and 12 motifs show enrichment uniquely present in class I, II and III
274 OCRs, respectively (Table 4). Genes that encode corresponding transcription factors for vast
275 majority of these motifs are found active in human myometrial tissues (Table S2), implicating

276 that interactions of these transcription factors with genomic DNA have a high probability to be
277 affected by change of chromatin structure during pregnancy.

278 Class I and III OCRs that are located within 25 kb of transcription start sites of DEGs are
279 arbitrarily defined as DEG-associated dynamic OCRs (Table 5), rendering these OCRs the
280 potential gene regulatory elements for linked DEGs subject to the control of chromatin structure
281 changes. Among the linked OCRs and DEGs, positive correlation is observed between 2989
282 OCRs and 1461 DEGs that have elevated gene expression concomitant with increased genome
283 accessibility or decreased gene expression with reduced genome accessibility (Table 5). This
284 observation suggests that these 2989 OCRs could function as putative enhancers for the 1461
285 associated DEGs. On the other hand, negative correlation is seen between 1660 OCRs and 980
286 DEGs that exhibit a reduction of gene expression with increased genome accessibility or an
287 increase of gene expression with decreased genome accessibility (Table 5). This inverse
288 correlation implicates a role of these 1660 OCRs as putative repressors for the 980 DEGs. Motif
289 enrichment analysis on the DEG-associated dynamic OCRs further reveals candidate
290 transcription regulators that may control transcription of the associated DEGs and whose actions
291 are possibly affected by change of chromatin structure over the course of pregnancy (Table S8).
292 Among the DNA-binding proteins that may occupy these enriched motifs, estrogen receptor,
293 glucocorticoid receptor, progesterone receptor, MEF2C, NFAT, NFkB, AP-1 and STAT
294 transcription factors have been studied for their roles in the myometrial biology [6, 51-54]; and
295 CTCF and YY1 are known for their functions in regulation of chromatin conformation [55, 56].
296 The presence of these motifs in the dynamic OCRs suggest that changes in chromatin structure
297 may also have an impact on the actions of these transcription and chromatin conformation
298 regulators in modulation of associated DEGs between the two states of pregnancy. Further
299 examining the associated DEGs by gene ontology enrichment analysis found signaling pathways
300 that are potentially subject to chromatin structural changes, including Rho family GTPases, actin
301 cytoskeleton, gap junction, eNOS, Relaxin, PDGF and HIPPO signaling for myometrial
302 remodeling and contraction regulation as well as glycolysis and Adrenomedullin for metabolism
303 and circulation control (Table 6 and Table S9). In summary, these findings identify potential
304 signaling pathways and their putative transcriptional regulators in the human myometrium that
305 may have an additional control mechanism through genome accessibility.

306 The ATAC-seq data also allows assessment of transcription factors' footprints in the open
307 chromatin regions. The bivariate genomic footprinting (BaGFoot) algorithm enables
308 identification of motifs that are located at the deepened protein-binding footprints (Δfootprint
309 depth) sites within the open chromatin regions of increasing DNA accessibility (Δflanking
310 accessibility) from one state to another [37]. The NP and TP myometrial tissues exhibit distinct
311 sets of enriched motifs (Figure S1 and Table S10). The corresponding transcription factors that
312 may occupy at these motifs and are also expressed ALX1, ARID3A, FOXC1, FOXJ2, FOXJ3,
313 HLF, HMGA1, HOXA13, HOXA5, HOXD9, NFIL3, NKX3.1, PBX1, POU6F1, PRRX2, REL
314 and TBP for the TP myometrium. In contrast, the expressing transcription regulators that may
315 bind at enriched motifs in the NP myometrium include EGR1, MDB2, MECP2, NRF1, SP1,
316 SP2, SP3, SP4, ZBTB7B, ZBTB4 and ZNF219. Our data suggest that the interactions between
317 these transcription factors and their genomic target sites in the myometrium are likely subject to
318 the change of chromatin structure at the epigenomic level transitioning toward term pregnancy.

319

320 PGR Genome Occupancy in the Myometrial Tissues

321 Since PGR plays a vital role in mediating the progesterone signaling and enrichment of its DNA
322 motif is found in the open chromatin regions of the myometrium, we next examine the
323 myometrial PGR genome occupancy profiles at both NP and TP stages. Myometrial biopsies
324 from two individual human subjects at each stage were subject to the PGR ChIP-seq assay. Peak
325 calling using data within each individual sample identifies 24095, 9778, 10717 and 8053 PGR
326 occupying intervals in NP1, NP2, TP1 and TP2 myometrial specimens, respectively, after
327 normalization to the same sequencing depth at 9 million reads per sample (Table S11). These
328 PGR binding regions presented in each stage account for 48.3% and 15.0% of open chromatin
329 regions in the NP and TP myometrium, respectively. PGR occupancy is enriched in promoters
330 and 5' untranslated regions (UTR) in all four myometrial specimens at the expense of the distal
331 intergenic areas (Table 7), implicating a close interaction between PGR and the transcription
332 machinery around the promoters *in vivo* for regulation of gene expression. Notably, the
333 enrichment of myometrial PGR occupancy around the promoter is most prominent in the
334 nonpregnant state (34.3% for NP1 and 35.4% for NP2). On the other hand, such enrichment is
335 relatively lower at the TP state (26.4% for TP1 and 12.0% for TP2) with comparatively higher

336 percentage of PGR binding in the distal intergenic region (Table 7). This finding indicates that
337 re-distribution of PGR genome occupancy occurs concurrently with myometrial remodeling and
338 transcriptomic changes in adaptation to pregnancy.

339 The DNA sequences of PGR occupying regions exhibited a significant enrichment of the
340 consensus PGR binding motif [57] in all four myometrial specimens in comparison with the
341 background genome (enrichment *p* value 1 x 10^{-18} [NP1], 1 x 10^{-686} [NP2], 1 x 10^{-1105} [TP1], 1 x
342 10^{-1059} [TP2], Table S12), while the PGR consensus motif can be found more frequently in the
343 TP than the NP myometrial PGR binding intervals (21.33% [TP1] and 26.20% [TP2] vs. 5.01%
344 [NP1] and 18.57% [NP2], Table S12). Over-representation of binding motifs for transcription
345 factors that have known indications in the myometrium is also seen across all myometrial
346 specimens, including NR3C1 (glucocorticoid receptor) [6, 58], ATF3 [59], FOSL1 [60], JUN
347 [60], KLF9 [61, 62], NF*k*B [63, 64] and STAT5 [54] (Table S12). Similarly, DNA binding
348 motifs for the PGR co-factor FOSL2 [27, 57], smooth muscle differentiation regulator TCF21
349 [65] and smooth muscle master regulator SRF (CArG)[66, 67] are over-represented throughout
350 the samples, too (Table S12). These data collectively show that the PGR may interact with DNA
351 via both consensus motif dependent and independent manners and such interaction is dynamic
352 during myometrial remodeling. Moreover, our *in vivo* observations provide clinical relevance to
353 previous *in vitro* findings that PGR interacts with other know myometrial and muscle
354 transcription factors in close proximity at cis-acting elements for regulation of myometrial
355 transcriptome.

356 Further examination of the motif enrichment data identifies candidate myometrial PGR-
357 partnering transcription factors, however, their functions in the myometrium await investigation.
358 The TEAD proteins are known to mediate the Hippo pathway for regulation of muscle fiber size
359 [68] and to interact with AP-1 factors for the smooth muscle fate decision [69]. The motif for
360 TEAD transcription factors is over-represented in PGR binding intervals across all four
361 specimens (Table S12) and expression of TEAD1, TEAD2, TEAD3 and TEAD4 is detected in
362 both NP and TP myometrial tissues (Table S2). The BATF family transcription factors function
363 as a pioneer factor that controls chromatin accessibility [70] and serve as co-regulators for PGR,
364 NR3C1 and AP-1 [71-73]. The binding motif for BATF, members of the AP-1 superfamily, is
365 among the top enriched motifs within PGR binding regions in all four myometrial samples

366 (Table S12) and BATF, BATF2 and BATF3 are all expressed in both stages of the examined
367 myometrium (Table S2). YY1, regulator of chromatin conformation and DNA looping [56]
368 exhibits adequate mRNA levels between NP and TP stages (Table S2). Interestingly, the YY1
369 binding motif is over-represented surrounding the PGR binding sites of NP myometrial samples
370 but becomes less enriched over background in the TP specimens (enrichment *p* value 1×10^{-55}
371 [NP1], 1×10^{-61} [NP2], 1×10^{-20} [TP1], > 0.01 [TP2], Table S12). These findings implicate
372 potential interactions of PGR with the Hippo signaling pathway, inflammatory response and
373 chromatin conformation regulators for transcription control *in vivo*. Furthermore, the example of
374 stage-associated differential enrichment of the YY1 motif in the PGR binding intervals suggest
375 that PGR may work with various sets of transcription factors to confer phenotype-specific
376 transcriptome profiles.

377 Next, we determine common and distinct PGR binding intervals between the NP and TP
378 myometrial samples. Union PGR binding peaks across samples were generated based on all PGR
379 binding intervals in four specimens to document the presence and absence of each PGR binding
380 site in individual specimens. Total 30613 union PGR binding peaks are found (Figure 5 and
381 Table S13). The numbers of union peaks present in each specimen are 24019, 9491, 10402 and
382 7928 for NP1, NP2, TP1 and TP3, respectively (Figure 5). NP1 and NP2 myometrial tissues
383 share 7323 union peaks while that number between TP1 and TP2 is 4839 (Figure 5). Among
384 these 7323 peaks in the NP myometrium, binding motifs of PGR, STAT transcription factors,
385 SRF, MyoD and SMAD2 are over-represented (Table 8 and Table S14). Enrichment of these
386 motifs are also found among the 4839 PGR occupying sites in the TP myometrium (Table 8 and
387 Table S14). Consistent with motif analysis results on individual specimens (Table S12), the PGR
388 consensus motif exhibits higher levels of enrichment in the PGR occupying intervals of the TP
389 myometrium in comparison with that of the NP stage (Table 8). In addition, STAT, CArG and
390 SMAD2 motifs also show increased enrichment in the TP myometrium while the MyoD motif
391 has stronger over-representation in NP specimens (Table 8 and Table S14). These observations
392 indicate adjustment of partnership with other transcription factors at different stages is a common
393 process among specimens beyond individual variations.

394 Further examining the stage-associated PGR occupying regions identified 2220 genomic regions
395 that are shared between the 7323 and 4839 PGR binding intervals while 2773 and 1047 have

396 distinct presence in NP and TP myometrium, respectively (Figure 5). In addition to differences in
397 genomic locations, the compositions of transcription factor binding motifs also show divergent
398 profiles among these three groups of PGR occupying regions (Table S15). Among the 95 motifs
399 that are compiled from the top 50 enriched motifs of each of the three groups, the enrichment p
400 values reveal a major difference on the extent of these motifs' presentation between the NP-
401 distinct and TP-distinct PGR occupying regions (Figure 6). The TP distinct regions are highly
402 enriched for the consensus binding motifs for progesterone and glucocorticoid receptors, AP-1
403 proteins and TEAD transcription factors, in contrast to the relatively lower enrichment in the NP
404 distinct regions. On the contrary, NP distinct sites show strong over-representations on motifs of
405 ETS transcription factors, nuclear transcription factor Y, CTCF, YY1, Sp1 and NRF1, which are
406 much less enriched in the TP distinct regions. Notably, the 2220 shared regions have a motif
407 enrichment profile similar to that of TP rather than NP distinct regions (Figure 6). This suggests
408 PGR at the NP stage may interact with a wider spectrum of transcription regulators while it
409 likely works with a more focused set of transcription factors in the TP myometrium. The data
410 collectively suggest that the dynamics of PGR binding locations between the two states of
411 myometrium allow various combinations of transcription factor binding motifs available for
412 corresponding regulators to interact with PGR at a state-specific manner.

413 Candidate PGR Direct Downstream Target Genes in the Myometrium

414 The association between the PGR genome occupancy and the myometrial transcriptome is
415 assessed by identifying the nearest genes to 2220 shared and 2773 and 1047 distinct PGR
416 binding intervals between the NP and TP myometrium. Among these 6040 PGR occupying
417 regions, 4355 (72%) are associated with 2203 myometrial active genes (Table 9 and Table S16).
418 These 2203 candidate PGR direct downstream target genes can be further sub-grouped into 1431
419 NP-distinct, 183 TP-distinct and 589 NP-TP shared active genes based on their association with
420 distinct or common PGR binding intervals (Table 9), in which Ingenuity Pathway Analysis
421 identified 51, 37 and 166 canonical signaling pathways, respectively, that have enrichment *p*
422 value less than 0.05 (Table S17). The top 50 associated pathways from each of the three groups
423 manifest divergent profiles (Figure 7). Notable example pathways that are selectively enriched in
424 individual groups include "estrogen receptor signaling" and "DNA Methylation and
425 Transcriptional Repression Signaling" for the NP distinct group, "IL-10 Signaling" and

426 “Inhibition of Matrix Metalloproteases” for the TP distinct group, and “Actin Cytoskeleton
427 Signaling” and “p53 Signaling” for the NP-TP shared group (Figure 7 and Table S17). In
428 contrast, no canonical pathway has the enrichment *p* value less than 0.05 across all three groups.
429 These findings suggest that each group of PGR binding regions may contribute to regulation of a
430 cohort of genes that cater to specific functions for physiological adaption on pregnancy.

431 PGR occupancy on genomic regions in association with genes of interest are further examined in
432 additional myometrial specimens, two each from NP and TP stages (Table 10). The glycolytic
433 genes *ENO1* and *LDHA* display reduced binding events in the TP myometrium compared with
434 that in NP. Given that both genes exhibit higher expression levels in the TP samples (Figure 3),
435 these findings together indicate a negative correlation between PGR occupancy and mRNA
436 levels. PLCL1 functions to attenuate prostaglandin-dependent calcium signaling (US Patent
437 20160161487A1). *PLCL1* is expressed in human myometrium (Figure 3 and Table S2) [40] and
438 is a PGR downstream target [74]. PGR occupancy in a region 93kb upstream of the *PLCL1* gene
439 can be detected in both cohorts of myometrial specimens (Table 10 and Table S13), which may
440 serve as a functional regulatory element for the myometrial *PLCL1* gene. While only a few
441 genomic regions were tested, the reproducible detection of PGR occupancy in different cohorts
442 of myometrial specimens validates the genome-wide ChIP-seq results. Moreover, these findings
443 also identified candidate cis-acting elements through which PGR may regulate expression of
444 glycolytic genes *ENO1* and *LDHA* as well as the contractility-associated gene *PLCL1*.

445

446 **Discussion**

447 Novelty of the study

448 The present study documents the molecular landscape of the NP and TP myometrium as well as
449 the changes between these two stages. While previous genome-wide studies identify candidate
450 mechanisms for the switch from nonlabor to labor states [40, 75, 76], results presented here
451 report the way the myometrium reorganizes and adapts from nonpregnant to gravid preceding the
452 switch for parturition. This is exemplified by the uniform increase of mRNA of parturition
453 associated genes *OXTR, GJA1, ZEB1* and *PLCL1* during myometrial remodeling followed by the
454 divergent change of expression patterns (Figure 1). Our transcriptome data broadens the

455 spectrum of the knowledge on myometrial gene expression dynamics and set the foundation for
456 future meta-analysis to understand the genetic program for myometrial remodeling during the
457 pregnancy cycle. The molecular pathways revealed here can also serve as a reference for
458 studying genetic and environmental impacts that derail normal pregnancy leading to disorders
459 such as preterm birth and dystocia.

460 The assessible genome maps offers a blueprint to study genetic and epigenetic regulation of the
461 myometrial transcriptome. The identified open chromatin regions likely house cis-acting
462 elements that participate in regulation of the myometrial transcriptome and they could be subject
463 to epigenetic control. For example, binding motifs of the estrogen receptor and the cell cycle
464 regulator E2F1 are over-represented in the open chromatin regions found only in the NP
465 myometrium (Table 4), which reflects the higher expression levels of genes for transcription and
466 gene control (Table 2) and implicates the preparation of smooth muscle proliferation for the early
467 gestation myometrial expansion under the control of estrogen receptor. Another example is the
468 parturition associated gene MEF2A [51]. Enrichment of the MEF2A binding motif in the class
469 III open chromatin regions (Table 4), suggest that accessibility of MEF2A to its target sites could
470 be another layer of regulation of its action in addition to changes in expression levels [51]. Our
471 genome-wide integrative analysis of genome accessibility and transcriptome have identified
472 potential regulatory elements and associated molecular pathways that may be affected the
473 chromatin accessibility (Table S8 and table S9). These findings pave the road for future in depth
474 study of the epigenetic impact on myometrial transcriptome changes.

475 Given that progesterone is the major steroid hormone for pregnancy and has a clinical indication
476 on preventing premature labor, the focused genome-wide myometrial PGR occupancy study
477 provides a map to identify PGR-associated cis-acting elements and their candidate downstream
478 target genes for further investigation on the mechanism of action of PGR. Notably, the impact of
479 losing uterine p53 on gestation length has been reported in the mouse model [49]. In our study,
480 the "p53 Signaling" is among the top enriched pathways in the putative PGR direct downstream
481 targets (Table S17). This finding suggests a potential interaction between PGR and p53 signaling
482 in the myometrium. Meanwhile, the over-represented transcription factor binding motifs
483 surrounding the PGR occupying sites suggest candidate PGR interacting partners for myometrial
484 gene regulation. For instance, the AP-1 proteins are known to partner with PGR for gene

485 regulation as exemplified by a few parturition maker genes [27]. We found that binding motifs of
486 many AP-1 subunits are among the top enriched motifs in the myometrial PGR occupying
487 regions (Table S14 and Figure 6), suggesting a potential genome-wide partnership between PGR
488 and AP-1. Our results not only provide human relevance to the known signaling pathways at the
489 *in vivo* level, but also allow identification of novel targets, either working with or under control
490 of PGR, for future research.

491 An Indication of Progesterone Receptor on Myometrial Metabolism and Remodeling

492 The elevated expression of genes for the glycolytic pathway and lactate production toward term
493 pregnancy have two physiological implications. First is the lactate production and the
494 myometrial contractility. Myometrial lactic acidosis is observed in women who have
495 dysfunctional labor [77]. It has been shown that acidic pH abrogates myometrial contraction
496 [78]. Lactate treatment can reduce spontaneous contraction [79] and suppresses uterine
497 inflammation and preterm birth [80]. Lactate is converted from the glycolysis product pyruvate
498 in the muscle system by the lactate dehydrogenase. Decreased muscle *Ldha* expression, which
499 encodes a subunit of the lactate dehydrogenase, leads to a reduction of pyruvate-to-lactate
500 conversion [81]. Our transcriptomic data indicates that the pathway for glycolysis and lactate
501 production is set for an increase of processing capacity toward term pregnancy (Figure 3 and
502 Table S2). Moreover, higher myometrial utilization of glucose at term pregnancy is also
503 supported by the change of expression pattern of glucose responsive genes (Table S4 and Table
504 S5). Our findings suggest that, during pregnancy, the myometrial transcriptome adapts to ramp
505 up the lactate production capacity, which contributes to maintaining the myometrial quiescence.
506 The second note is on the energy metabolism and molecular biosynthesis. Our transcriptomic
507 data shows that, in the TP myometrium, an increase of HIF1A molecular activity likely occurs
508 based on the expression pattern of HIF1A downstream targets (Table S4 and Table S5). The rise
509 of HIF1A activity suggests a hypoxic myometrium at term. Under the anaerobic condition,
510 increased glycolysis can generate ATP to compensate the need of energy for maintaining cellular
511 functions. On the other hand, at normoxia, the increased capacity for higher flux of glycolysis
512 can supply the intermediates for amino acid synthesis to generate building blocks for myometrial
513 expansion over the course of pregnancy. The increased glycolytic gene expression at pregnancy
514 would fit these hypotheses for the change of myometrial functions (Figure 3). Lastly, the binding

515 of PGR in the genomic loci of ENO1 and LDHA links PGR to the regulation of myometrial
516 metabolism (Table 10), which awaits further investigation.

517 Limitation and future direction

518 The resolution of molecular profiling data and integration of multiomics information are the two
519 major limitations exist in the present study. The genome-wide data here is a summary
520 observation of many cells that reside in pieces of myometrial tissues. While the smooth muscle
521 cells make up the majority of the mass, readings from other cell type such as blood and vascular
522 cells are also incorporated as part of the summary results, which may reduce the signal-to-noise
523 ratio of the information on the cell type of interest. Despite potential contribution of other cell
524 type transcripts, the myometrial transcriptome data exhibits a strong association with known
525 smooth muscle and myometrial programs (Table 2 and Table 3), the ATACseq data establishes
526 close links between putative cis-acting elements and signaling pathways for muscle functions
527 (Table 6), and the PGR cistrome data detects enrichment of binding motifs for smooth muscle
528 master regulators SRF and MyoD (Table 8). These examples demonstrate that the current data
529 can provide significant information to support existing knowledge and supply novel findings.
530 The emerging molecular profiling assays at the single cell level would provide a greater
531 resolution than current results obtained with more established technology, leading to further
532 dissection of each cell's role and the underlying molecular events in a given myometrial state.

533 Another limitation on the data resolution is that the antibody used for generating the current PGR
534 ChIPseq results detects both major PGR isoforms in the myometrium, the PGR-A and PGR-B.
535 These two PGR isoforms differ in the AF-3 transactivation domain that only exists in the PGR-
536 B. Both isoforms are functionally capable of modulating transcription of common and distinct
537 sets of downstream genes depending on the context [25]. Therefore, the stoichiometric ratio
538 between the two isoforms in different stages of myometrium needs to be factored into
539 intepretation of the effect of PGR on expression of associated genes. For studies on human
540 tissues, there is an urgent need to develop the isoform-specific antibodies for PGR, perhaps
541 through targeting the protein domains with isoform-specific conformations.

542 With respect to the limitation on integration of multiomics information, in this manuscript the
543 PGR occupancy and myometrial transcriptome association study is based on a stringent criterion
544 that only link one nearest gene to each individual PGR occupying site (Table 9). The rationale to

use such as stringent criterion is based on the observation that majority of the PGR occupying sites are located near gene bodies (Table 7). PGR occupied cis-acting elements likely impose a greater influence on the myometrial transcriptome according to emerging transcription control models that each gene is subject to regulation by multiple enhancers and vice versa in a topological associated domain formed via chromatin conformation [82, 83]. Future integration of chromatin conformation data, generated from the high throughput chromatin conformation assay, would better assign PGR binding cis-acting elements with associated genes, especially on the long-distance interactions, to provide correlation information closer to the true molecular events.

Acknowledgement

This work was supported by the Intramural Research Program of the National Institutes of Health: Project Z1AES103311-01 and March of Dime. We thank the NIEHS Epigenomics and DNA Sequencing Core Laboratory for the technical assistance and Ms. Sylvia Hewitt for critical commenting.

Author Contribution

SPW and FJD designed and wrote the manuscript. MLA obtained permission from the Institutional Review Board to perform all work, collected the patient consents and myometrial specimens and wrote the corresponding section of the Methods section. SPW, OME and XL performed experiments and associated data analysis. TW, LZ and SPW conducted bioinformatic analyses. TW and LZ wrote the bioinformatic part of the Methods section.

Figure Legend

Figure 1. mRNA levels of parturition related genes in nonpregnant and term pregnant myometrium. Relative mRNA levels by qRT-PCR from myometrial tissues of 6 (NP, dots) and 9 (TP, triangles) human subjects. The Y-axis denotes relative mRNA levels. *, $p < 0.05$ by two-tailed t-test. Orange bars denote the mean of each group.

572 **Figure 2. Differences between NP and TP myometrial tissues at the transcriptomic level.**
573 (A) Principle Component Analysis of NP (blue) and TP (red) Transcriptome. (B) Differentially
574 expressed genes (DEGs) between groups. Differentially expressed genes are defined as absolute
575 fold change ≥ 1.4, adjusted *p*-value < 0.05 and having FPKM ≥ 1 in at least one of the samples.

576 **Figure 3. Expression of glycolytic genes**. The diagram to the left depicts the glycolysis
577 pathway. (A) RNAseq results. Yellow and blue depict high and low levels of gene expression,
578 respectively. (B-H) Relative mRNA levels of tissues from the same cohort of human subjects as
579 depicted in figure 1. The Y-axis denotes relative mRNA levels. *, $p < 0.05$ by two-tailed t-test.
580 Orange bars denote the mean of each group. N=6 for NP and 9 for TP.

581 **Figure 4. Open chromatin region in the myometrium.** Numbers of open chromatin regions
582 (OCRs) identified in 3 NP and 3 TP specimens by ATAC-seq. OCRs within each group were
583 pooled together. Numbers of shared and unique OCRs between NP and TP samples are also
584 noted.

585 **Figure 5. Number of PGR occupying regions in the genome of the human myometrium.**
586 PGR ChIP-seq was performed in two separate specimens at either NP or TP stages. The flower
587 Venn diagram illustrates the numbers of overlapping and distinct PGR occupying sites among
588 the four specimens.

589 **Figure 6. Top enriched transcription factor binding motifs in 2773 NP distinct (NPD), 1047**
590 **TP distinct (TPD) and 2220 NP-TP shared (S) PGR occupying sites**. Top 50 motifs from each
591 group are compiled and displayed with log p values. Color codes are depicted with the red-white-
592 blue pattern with red showing the strongest enrichment and blue being the least enriched.

593 **Figure 7. Top enriched canonical pathways in 1431 NP-distinct (NPD), 183 TP-distinct**
594 **(TPD) and 589 NP-TP shared (S), PGR-linked active genes**. Top 50 enriched pathways from
595 the Ingenuity Pathway Analysis from each group are compiled and displayed with log p values.
596 Color codes are depicted with the red-white-blue pattern with red showing the strongest
597 enrichment and blue being the least enriched.

598 **Figure S1.** Bag plot depicting change of DNA accessibility (ΔFA) and alteration in the depth of
599 protein-binding footprints (ΔFPD) from the NP to the TP stages. Motifs with statistical
600 significance are labeled in red squares.

601

602 **Table Legend**

603 **Table 1.** Transcriptome of Human myometrium in Non-pregnant (NP) and Term-pregnant (TP)
604 human subjects. Genes with FPKM ≥ 1 in at least one of the specimens within each group are
605 defined as expressed.

606 **Table 2**. Enriched Gene Ontology terms in differentially expressed genes (DEGs) between NP
607 and TP myometrium.

608 **Table 3.** Changes of molecular activities from NP to TP predicted by Ingenuity Pathway
609 Analysis (IPA) based on human RNAseq and mouse microarray (GSE17021, virgin vs. 18.5 dpc
610 myometrium) results.

611 **Table 4.** Enriched motifs in each class of open chromatin regions.

612 **Table 5. Association between DEGs and dynamic OCRs.** Class I and III open chromatin
613 regions are defined as DEG-associated if they are located within 25kb of the transcription start
614 site of DEGs. Positive correlation is defined if 1. increased gene expression and genome
615 accessibility at associated open chromatin regions or 2. decreased gene expression and genome
616 accessibility at associated open chromatin regions. Negative correlation is defined if 1. decreased
617 gene expression and increased genome accessibility at associated open chromatin regions or 2.
618 increased gene expression and decreased genome accessibility at associated open chromatin
619 regions. All comparisons were made by TP over NP.

620 **Table 6.** Selected Pathways Associated with Changes of the Open Chromatin Status. IPA
621 Canonical Pathways Analysis.

622 **Table 7. Genome-wide PGR occupying sites relative to gene bodies.** PGR binding intervals
623 were annotated by the Cis-regulatory Element Annotation System. The promoter is defined as a
624 region within 3 kb upstream of the transcription start site. The downstream of gene body refers to
625 an interval within 3 kb downstream of the transcription termination site.

626 **Table 8.** Selected Enriched motifs in common PGR-binding intervals at each stage.

627 **Table 9.** The association between PGR occupancy and myometrial active genes. A list of nearest
628 genes to the 2220, 7323 and 4839 shared and distinct PGR occupying intervals was identified
629 and further filtered with the criteria of having the maximum FPKM value greater or equal than 1
630 among the 6 myometrial RNAseq samples to catalog the PGR-associated active genes.

631 **Table 10.** PGR occupancy at selected genomic loci in a second cohort of myometrial specimens.
632 ChIP-qPCR was performed in a separate set of NP (n=2) and TP (n=2) myometrial tissues for
633 PGR occupancy test. Technical triplicates for each qPCR reaction was performed and the mean
634 and the standard deviation of triplicates was used for calculation of PGR binding events. Untr12
635 located in a gene desert serves as a negative control.

636 **Table S1**. List of human myometrial specimens.

637 **Table S2.** Active Genes in Human Myometrium

638 **Table S3.** A complete list of Gene Ontology analysis of Table 2.

639 **Table S4**. Predicted molecular activities by Ingenuity Pathway Analysis Differentially Expressed
640 Genes between NP and TP human myometrium.

641 **Table S5**. Predicted molecular activities by Ingenuity Pathway Analysis on Differentially
642 Expressed Genes between 18.5dpc and virgin mouse myometrium (GSE17021).

643 **Table S6.** Genome coordinates of open chromatin regions in human myometrial specimens. "1"
644 and "0" represent presence and absence, respectively, in the NP and TP myometrium. Classes are
645 defined in Figure 4.

646 **Table S7.** Motif enrichment analysis by HOMER known motif in the three classes of open
647 chromatin regions that are defined in Figure 4.

648 **Table S8.** Motif enrichment analysis on the DEG-associated dynamic OCRs

649 **Table S9.** Canonical Pathways that are linked to dynamic OCRs associated DEGs.

650 **Table S10.** Transcription footprinting assessment in the NP and TP myometrial specimens by
651 BaGFoot.

652 **Table S11.** Genome coordinates (Hg19) of PGR occupying intervals in myometrial tissues of
653 four human subjects.

654 **Table S12.** Enriched motifs in each individual myometrial specimen. Data is from the output
655 files of the HOMER unkown motif search algorithm.

656 **Table S13.** Union peak information of PGR binding intervals across all four myometrial
657 specimens. In the "UnionPeak-vs-Sample" section, 1 and 0 denote presence and absence of the
658 PGR binding peak in each individual specimen.

659 **Table S14.** Enrichment analysis on 428 transcription factor binding motifs in common PGR
660 occupying sites within each stage of myometrial specimens.

661 **Table S15.** Enrichment analysis on 428 known transcription factor binding motifs in shared and
662 distinct PGR occupying regions between NP and TP groups.

663 **Table S16.** Association between PGR occupancy and myometrial active genes

664 **Table S17.** Canonical pathways in association with PGR occupancy and myometrial active
665 genes. 1431, 589 and 183 active genes that are linked to NP-distinct, NP-TP shared and TP-
666 distinct PGR occupying sites, as depicted in Table 9, were subject to Ingenuity Pathway
667 Analysis.

668

669 **References**

670 1. Shynlova, O., et al., *Myometrial apoptosis: activation of the caspase cascade in the pregnant rat*
671 *myometrium at midgestation.* Biol Reprod, 2006. **74**(5): p. 839-49.
672 2. Shynlova, O., R. Kwong, and S.J. Lye, *Mechanical stretch regulates hypertrophic phenotype of*
673 *the myometrium during pregnancy.* Reproduction, 2010. **139**(1): p. 247-53.
674 3. Garfield, R.E. and W.L. Maner, *Physiology and electrical activity of uterine contractions.* Semin
675 Cell Dev Biol, 2007. **18**(3): p. 289-95.
676 4. Noakes, D.E., *7 - Physiology of the Puerperium*, in *Veterinary Reproduction and Obstetrics*
677 *(Tenth Edition)*, D.E. Noakes, T.J. Parkinson, and G.C.W. England, Editors. 2019, W.B.
678 Saunders: St. Louis (MO). p. 148-156.
679 5. Kyathanahalli, C., et al., *Cross-species withdrawal of MCL1 facilitates postpartum uterine*
680 *involution in both the mouse and baboon.* Endocrinology, 2013. **154**(12): p. 4873-84.
681 6. Whirledge, S., D. Dixon, and J.A. Cidlowski, *Glucocorticoids regulate gene expression and*
682 *repress cellular proliferation in human uterine leiomyoma cells.* Horm Cancer, 2012. **3**(3): p. 79-
683 92.
684 7. Welsh, T., et al., *Estrogen receptor (ER) expression and function in the pregnant human*
685 *myometrium: estradiol via ERalpha activates ERK1/2 signaling in term myometrium.* J
686 Endocrinol, 2012. **212**(2): p. 227-38.
687 8. Anamthathmakula, P., et al., *Estrogen receptor alpha isoform ERdelta7 in myometrium*
688 *modulates uterine quiescence during pregnancy.* EBioMedicine, 2019. **39**: p. 520-530.

689 9. Stanfield, Z., et al., *Interplay of transcriptional signaling by progesterone, cyclic AMP, and*
690 *inflammation in myometrial cells: implications for the control of human parturition.* Mol Hum
691 Reprod, 2019. **25**(7): p. 408-422.
692 10. Lee, Y., et al., *Interactions between inflammatory signals and the progesterone receptor in*
693 *regulating gene expression in pregnant human uterine myocytes.* J Cell Mol Med, 2012. **16**(10):
694 p. 2487-503.
695 11. Jaffer, S., O. Shynlova, and S. Lye, *Mammalian target of rapamycin is activated in association*
696 *with myometrial proliferation during pregnancy.* Endocrinology, 2009. **150**(10): p. 4672-80.
697 12. Ciarmela, P., et al., *Presence, Actions, and Regulation of Myostatin in Rat Uterus and*
698 *Myometrial Cells.* Endocrinology, 2009. **150**(2): p. 906-914.
699 13. Ono, M., et al., *CD34 and CD49f Double-Positive and Lineage Marker-Negative Cells Isolated*
700 *from Human Myometrium Exhibit Stem Cell-Like Properties Involved in Pregnancy-Induced*
701 *Uterine Remodeling.* Biol Reprod, 2015. **93**(2): p. 37.
702 14. Ono, M., et al., *Paracrine activation of WNT/beta-catenin pathway in uterine leiomyoma stem*
703 *cells promotes tumor growth.* Proc Natl Acad Sci U S A, 2013. **110**(42): p. 17053-8.
704 15. Lee, W.S., et al., *Progesterone inhibits arterial smooth muscle cell proliferation.* Nat Med, 1997.
705 **3**(9): p. 1005-8.
706 16. Lydon, J.P., et al., *Mice lacking progesterone receptor exhibit pleiotropic reproductive*
707 *abnormalities.* Genes Dev, 1995. **9**(18): p. 2266-78.
708 17. Longenecker, J.P., L.A. Kilty, and L.K. Johnson, *Glucocorticoid inhibition of vascular smooth*
709 *muscle cell proliferation: influence of homologous extracellular matrix and serum mitogens.* J
710 Cell Biol, 1984. **98**(2): p. 534-40.
711 18. Roth, M., et al., *Dysfunctional interaction of C/EBPalpha and the glucocorticoid receptor in*
712 *asthmatic bronchial smooth-muscle cells.* N Engl J Med, 2004. **351**(6): p. 560-74.
713 19. Navathe, R. and V. Berghella, *Progesterone as a tocolytic agent for preterm labor: a systematic*
714 *review.* Curr Opin Obstet Gynecol, 2016. **28**(6): p. 464-469.
715 20. Li, Q., et al., *Chronic Exposure to Bisphenol A Affects Uterine Function During Early Pregnancy*
716 *in Mice.* Endocrinology, 2016. **157**(5): p. 1764-74.
717 21. Bhurke, A.S., I.C. Bagchi, and M.K. Bagchi, *Progesterone-Regulated Endometrial Factors*
718 *Controlling Implantation.* Am J Reprod Immunol, 2016. **75**(3): p. 237-45.
719 22. Grimm, S.L., S.M. Hartig, and D.P. Edwards, *Progesterone Receptor Signaling Mechanisms.* J
720 Mol Biol, 2016. **428**(19): p. 3831-49.
721 23. Renthal, N.E., et al., *Molecular Regulation of Parturition: A Myometrial Perspective.* Cold
722 Spring Harb Perspect Med, 2015. **5**(11).
723 24. Wu, S.P. and F.J. DeMayo, *Progesterone Receptor Signaling in Uterine Myometrial Physiology*
724 *and Preterm Birth.* Curr Top Dev Biol, 2017. **125**: p. 171-190.
725 25. Patel, B., et al., *Role of nuclear progesterone receptor isoforms in uterine pathophysiology.* Hum
726 Reprod Update, 2015. **21**(2): p. 155-73.
727 26. Amini, P., et al., *Progesterone and cAMP synergize to inhibit responsiveness of myometrial cells*
728 *to pro-inflammatory/pro-labor stimuli.* Mol Cell Endocrinol, 2019. **479**: p. 1-11.
729 27. Nadeem, L., et al., *Molecular evidence of functional progesterone withdrawal in human*
730 *myometrium.* Nat Commun, 2016. **7**: p. 11565.
731 28. Nadeem, L., et al., *Progesterone Via its Type-A Receptor Promotes Myometrial Gap Junction*
732 *Coupling.* Sci Rep, 2017. **7**(1): p. 13357.
733 29. Merlino, A.A., et al., *Nuclear progesterone receptors in the human pregnancy myometrium:*
734 *evidence that parturition involves functional progesterone withdrawal mediated by increased*
735 *expression of progesterone receptor-A.* J Clin Endocrinol Metab, 2007. **92**(5): p. 1927-33.
736 30. Trapnell, C., L. Pachter, and S.L. Salzberg, *TopHat: discovering splice junctions with RNA-Seq.*
737 Bioinformatics, 2009. **25**(9): p. 1105-11.

738 31. Trapnell, C., et al., *Transcript assembly and quantification by RNA-Seq reveals unannotated*
739 *transcripts and isoform switching during cell differentiation.* Nat Biotechnol, 2010. **28**(5): p. 511-
740 5.
741 32. Huang da, W., B.T. Sherman, and R.A. Lempicki, *Systematic and integrative analysis of large*
742 *gene lists using DAVID bioinformatics resources.* Nat Protoc, 2009. **4**(1): p. 44-57.
743 33. Huang da, W., B.T. Sherman, and R.A. Lempicki, *Bioinformatics enrichment tools: paths toward*
744 *the comprehensive functional analysis of large gene lists.* Nucleic Acids Res, 2009. **37**(1): p. 1-
745 13.
746 34. Langmead, B., et al., *Ultrafast and memory-efficient alignment of short DNA sequences to the*
747 *human genome.* Genome Biol, 2009. **10**(3): p. R25.
748 35. Zhang, Y., et al., *Model-based analysis of ChIP-Seq (MACS).* Genome Biol, 2008. **9**(9): p. R137.
749 36. Heinz, S., et al., *Simple combinations of lineage-determining transcription factors prime cis-*
750 *regulatory elements required for macrophage and B cell identities.* Mol Cell, 2010. **38**(4): p. 576-
751 89.
752 37. Baek, S., I. Goldstein, and G.L. Hager, *Bivariate Genomic Footprinting Detects Changes in*
753 *Transcription Factor Activity.* Cell Rep, 2017. **19**(8): p. 1710-1722.
754 38. Bentley, D.R., et al., *Accurate whole human genome sequencing using reversible terminator*
755 *chemistry.* Nature, 2008. **456**(7218): p. 53-9.
756 39. Quinlan, A.R. and I.M. Hall, *BEDTools: a flexible suite of utilities for comparing genomic*
757 *features.* Bioinformatics, 2010. **26**(6): p. 841-2.
758 40. Chan, Y.W., et al., *Assessment of myometrial transcriptome changes associated with spontaneous*
759 *human labour by high-throughput RNA-seq.* Exp Physiol, 2014. **99**(3): p. 510-24.
760 41. Chow, L. and S.J. Lye, *Expression of the gap junction protein connexin-43 is increased in the*
761 *human myometrium toward term and with the onset of labor.* Am J Obstet Gynecol, 1994. **170**(3):
762 p. 788-95.
763 42. Kimura, T., et al., *Expression of oxytocin receptor in human pregnant myometrium.*
764 Endocrinology, 1996. **137**(2): p. 780-5.
765 43. Renthal, N.E., et al., *miR-200 family and targets, ZEB1 and ZEB2, modulate uterine quiescence*
766 *and contractility during pregnancy and labor.* Proc Natl Acad Sci U S A, 2010. **107**(48): p.
767 20828-33.
768 44. Gao, Y., et al., *Constitutive activation of transforming growth factor Beta receptor 1 in the mouse*
769 *uterus impairs uterine morphology and function.* Biol Reprod, 2015. **92**(2): p. 34.
770 45. Li, Q., et al., *Transforming growth factor beta receptor type 1 is essential for female reproductive*
771 *tract integrity and function.* PLoS Genet, 2011. **7**(10): p. e1002320.
772 46. Oldenhof, A.D., et al., *Mitogen-activated protein kinases mediate stretch-induced c-fos mRNA*
773 *expression in myometrial smooth muscle cells.* Am J Physiol Cell Physiol, 2002. **283**(5): p.
774 C1530-9.
775 47. Li, Y., et al., *Focal adhesion signaling is required for myometrial ERK activation and contractile*
776 *phenotype switch before labor.* J Cell Biochem, 2007. **100**(1): p. 129-40.
777 48. Akerman, A.W., et al., *Elevated Wall Tension Initiates Interleukin-6 Expression and Abdominal*
778 *Aortic Dilation.* Ann Vasc Surg, 2018. **46**: p. 193-204.
779 49. Hirota, Y., et al., *Uterine-specific p53 deficiency confers premature uterine senescence and*
780 *promotes preterm birth in mice.* J Clin Invest, 2010. **120**(3): p. 803-15.
781 50. Buenrostro, J.D., et al., *Transposition of native chromatin for fast and sensitive epigenomic*
782 *profiling of open chromatin, DNA-binding proteins and nucleosome position.* Nat Methods, 2013.
783 **10**(12): p. 1213-8.
784 51. Ackerman, W.E.t., et al., *Integrated microRNA and mRNA network analysis of the human*
785 *myometrial transcriptome in the transition from quiescence to labor.* Biol Reprod, 2018.
786 52. Khanjani, S., et al., *NFkappaB and AP-1 drive human myometrial IL8 expression.* Mediators
787 Inflamm, 2012. **2012**: p. 504952.

53. Pont, J.N., C.A. McArdle, and A. Lopez Bernal, *Oxytocin-stimulated NFAT transcriptional activation in human myometrial cells.* Mol Endocrinol, 2012. **26**(10): p. 1743-56.
54. Williams, K.C., et al., *MicroRNA-200a serves a key role in the decline of progesterone receptor function leading to term and preterm labor.* Proc Natl Acad Sci U S A, 2012. **109**(19): p. 7529-34.
55. Ghirlando, R. and G. Felsenfeld, *CTCF: making the right connections.* Genes Dev, 2016. **30**(8): p. 881-91.
56. Weintraub, A.S., et al., *YY1 Is a Structural Regulator of Enhancer-Promoter Loops.* Cell, 2017. **171**(7): p. 1573-1588 e28.
57. Mazur, E.C., et al., *Progesterone receptor transcriptome and cistrome in decidualized human endometrial stromal cells.* Endocrinology, 2015. **156**(6): p. 2239-53.
58. Lei, K., et al., *Progesterone acts via the nuclear glucocorticoid receptor to suppress IL-1beta-induced COX-2 expression in human term myometrial cells.* PLoS One, 2012. **7**(11): p. e50167.
59. Payson, M., et al., *Activating transcription factor 3 gene expression suggests that tissue stress plays a role in leiomyoma development.* Fertil Steril, 2009. **92**(2): p. 748-55.
60. Nadeem, L., et al., *Differential expression of myometrial AP-1 proteins during gestation and labour.* J Cell Mol Med, 2017.
61. Zeng, Z., et al., *Delayed parturition and altered myometrial progesterone receptor isoform A expression in mice null for Kruppel-like factor 9.* Biol Reprod, 2008. **78**(6): p. 1029-37.
62. Pabona, J.M., et al., *Prolonged pregnancy in women is associated with attenuated myometrial expression of progesterone receptor co-regulator Kruppel-like Factor 9.* J Clin Endocrinol Metab, 2015. **100**(1): p. 166-74.
63. Hardy, D.B., et al., *Progesterone receptor plays a major antiinflammatory role in human myometrial cells by antagonism of nuclear factor-kappaB activation of cyclooxygenase 2 expression.* Mol Endocrinol, 2006. **20**(11): p. 2724-33.
64. MacIntyre, D.A., et al., *Activator protein 1 is a key terminal mediator of inflammation-induced preterm labor in mice.* FASEB J, 2014. **28**(5): p. 2358-68.
65. Zhao, Q., et al., *TCF21 and AP-1 interact through epigenetic modifications to regulate coronary artery disease gene expression.* Genome Med, 2019. **11**(1): p. 23.
66. McDonald, O.G. and G.K. Owens, *Programming smooth muscle plasticity with chromatin dynamics.* Circ Res, 2007. **100**(10): p. 1428-41.
67. Gualdrini, F., et al., *SRF Co-factors Control the Balance between Cell Proliferation and Contractility.* Mol Cell, 2016. **64**(6): p. 1048-1061.
68. Watt, K.I., et al., *The Hippo pathway effector YAP is a critical regulator of skeletal muscle fibre size.* Nat Commun, 2015. **6**: p. 6048.
69. Joshi, S., et al., *TEAD transcription factors are required for normal primary myoblast differentiation in vitro and muscle regeneration in vivo.* PLoS Genet, 2017. **13**(2): p. e1006600.
70. Karwacz, K., et al., *Critical role of IRF1 and BATF in forming chromatin landscape during type 1 regulatory cell differentiation.* Nat Immunol, 2017. **18**(4): p. 412-421.
71. Hill, K.K., et al., *A progesterone receptor co-activator (JDP2) mediates activity through interaction with residues in the carboxyl-terminal extension of the DNA binding domain.* J Biol Chem, 2009. **284**(36): p. 24415-24.
72. Wardell, S.E., et al., *Jun dimerization protein 2 functions as a progesterone receptor N-terminal domain coactivator.* Mol Cell Biol, 2002. **22**(15): p. 5451-66.
73. Birth, P., et al., *Identification and characterization of BATF3 as a context-specific coactivator of the glucocorticoid receptor.* PLoS One, 2017. **12**(7): p. e0181219.
74. Muter, J., et al., *Progesterone-Dependent Induction of Phospholipase C-Related Catalytically Inactive Protein 1 (PRIP-1) in Decidualizing Human Endometrial Stromal Cells.* Endocrinology, 2016. **157**(7): p. 2883-93.
75. Stanfield, Z., et al., *Myometrial Transcriptional Signatures of Human Parturition.* Front Genet, 2019. **10**: p. 185.

839 76. Mittal, P., et al., *Characterization of the myometrial transcriptome and biological pathways of*
840 *spontaneous human labor at term.* J Perinat Med, 2010. **38**(6): p. 617-43.
841 77. Quenby, S., et al., *Dysfunctional labor and myometrial lactic acidosis.* Obstet Gynecol, 2004.
842 **103**(4): p. 718-23.
843 78. Parratt, J., M. Taggart, and S. Wray, *Abolition of contractions in the myometrium by acidification*
844 *in vitro.* Lancet, 1994. **344**(8924): p. 717-8.
845 79. Hanley, J.A., A. Weeks, and S. Wray, *Physiological increases in lactate inhibit intracellular*
846 *calcium transients, acidify myocytes and decrease force in term pregnant rat myometrium.* J
847 Physiol, 2015. **593**(20): p. 4603-14.
848 80. Madaan, A., et al., *Lactate produced during labor modulates uterine inflammation via*
849 *GPR81 (HCA1).* American Journal of Obstetrics and Gynecology, 2017. **216**(1): p. 60.e1-60.e17.
850 81. Summermatter, S., et al., *Skeletal muscle PGC-1alpha controls whole-body lactate homeostasis*
851 *through estrogen-related receptor alpha-dependent activation of LDH B and repression of LDH*
852 *A.* Proc Natl Acad Sci U S A, 2013. **110**(21): p. 8738-43.
853 82. Hnisz, D., D.S. Day, and R.A. Young, *Insulated Neighborhoods: Structural and Functional Units*
854 *of Mammalian Gene Control.* Cell, 2016. **167**(5): p. 1188-1200.
855 83. Medina-Rivera, A., et al., *Widespread Enhancer Activity from Core Promoters.* Trends Biochem
856 Sci, 2018. **43**(6): p. 452-468.

857

Figure 1

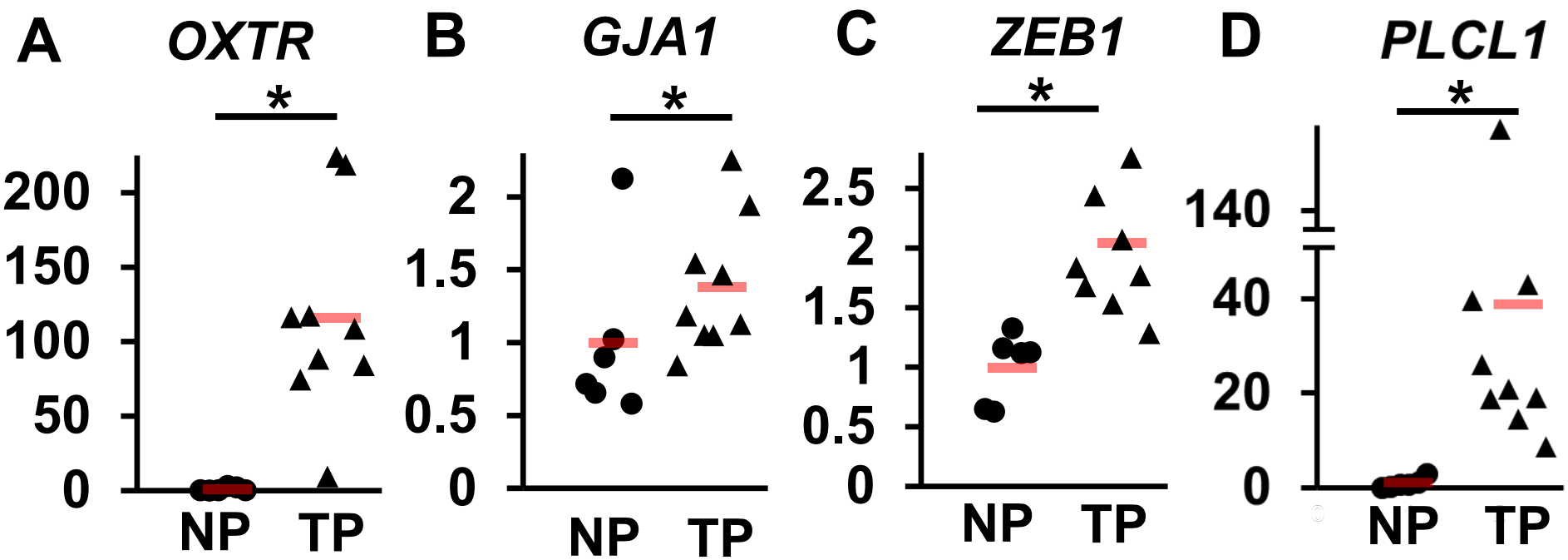
A
OXTR
*
200
150
100
50
0
NP
TP
B
GJA1
*
2
1.5
1
0.5
0
NP
TP
C
ZEB1
*
2.5
2
1.5
1
0.5
0
NP
TP
D
PLCL1
*
140
40
20
0
NP
TP

Figure 2

A

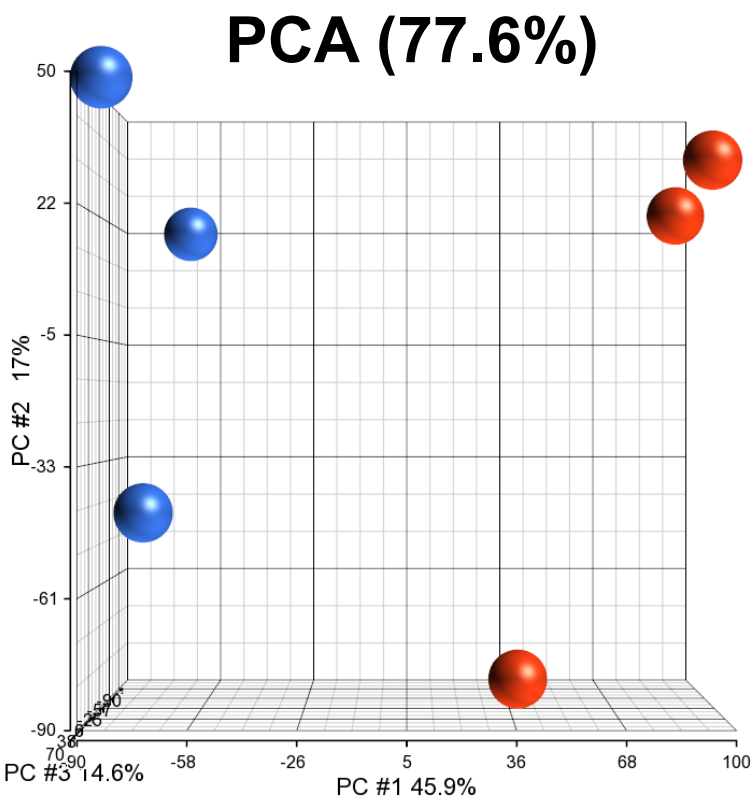
PCA (77.6%)
50
22
-5
-33
-61
-90
PC #2 17%
-90
-58
-26
5
36
68
100
PC #1 45.9%

B

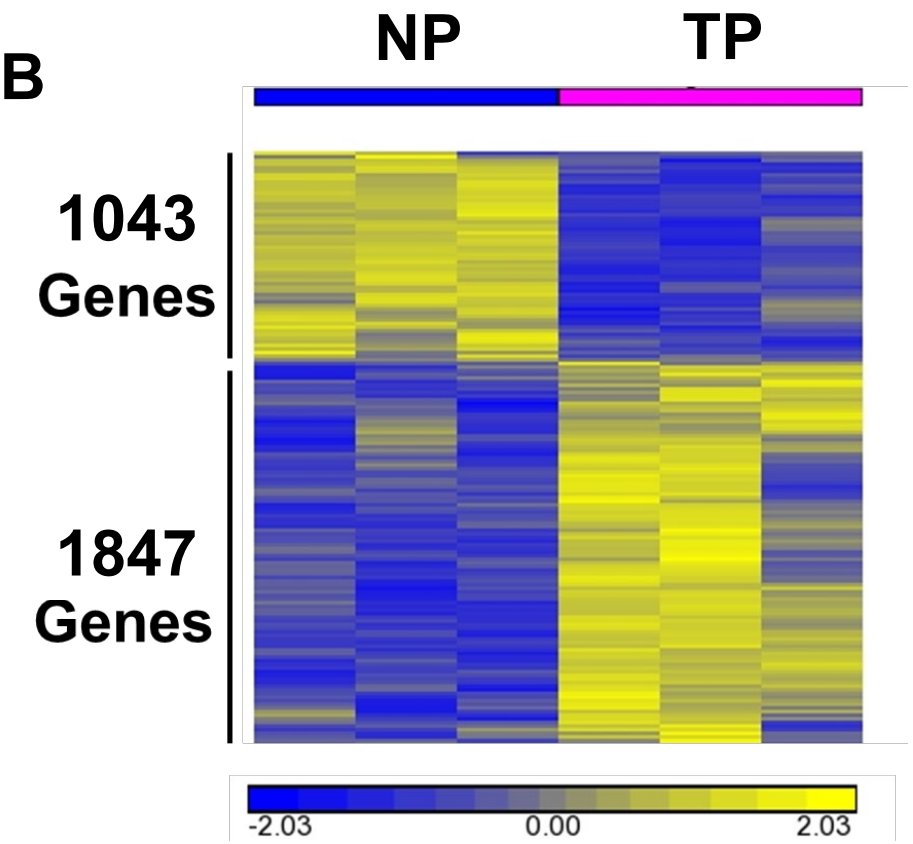
NP
TP
1043
Genes
1847
Genes
-2.03
0.00
2.03

Figure 3

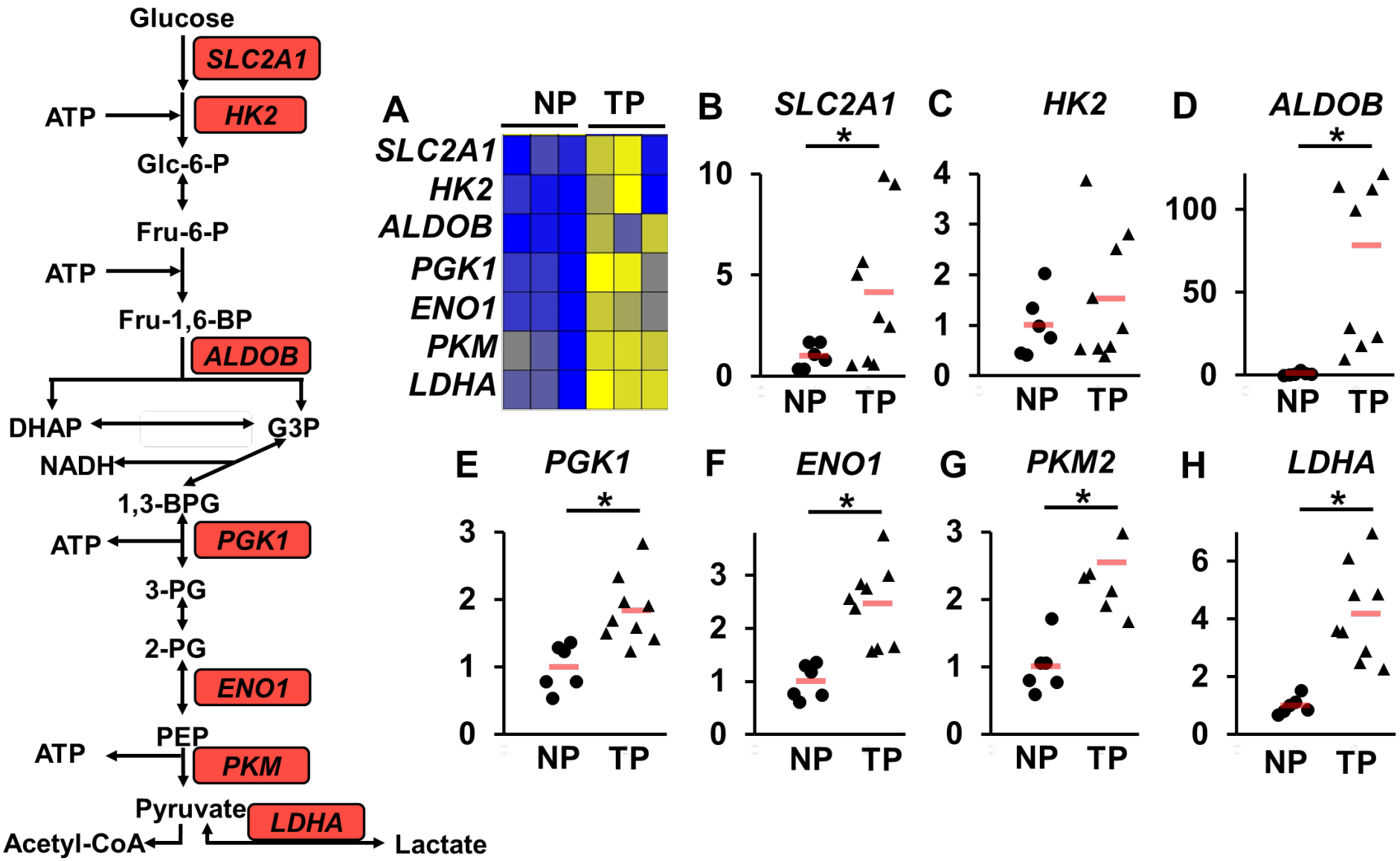
Glucose
SLC2A1
ATP
HK2
Glc-6-P
Fru-6-P
ATP
Fru-1,6-BP
ALDOB
DHAP
G3P
NADH
1,3-BPG
ATP
PGK1
3-PG
2-PG
ENO1
PEP
ATP
PKM
Pyruvate
LDHA
Acetyl-CoA
Lactate
A
NP
TP
SLC2A1
HK2
ALDOB
PGK1
ENO1
PKM
LDHA
B
SLC2A1
C
HK2
D
ALDOB
E
PGK1
F
ENO1
G
PKM2
H
LDHA
*
NP
TP

Figure 4

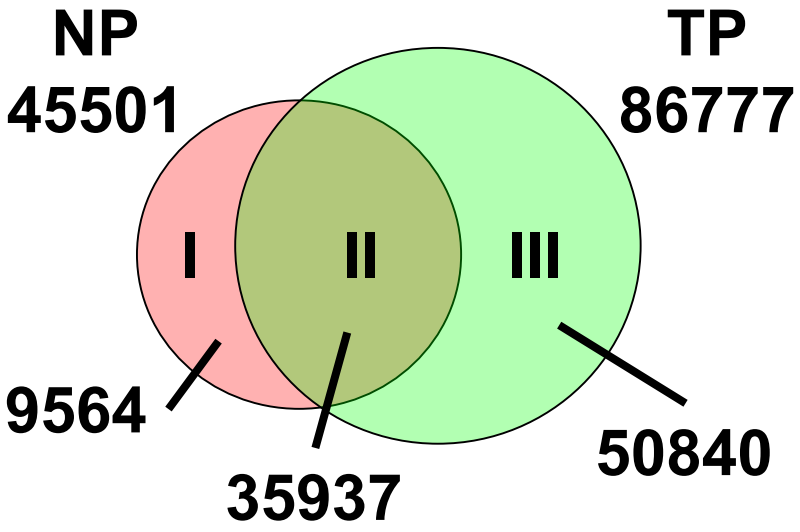

Figure 5

Number of PGR occupying regions in the human myometrium

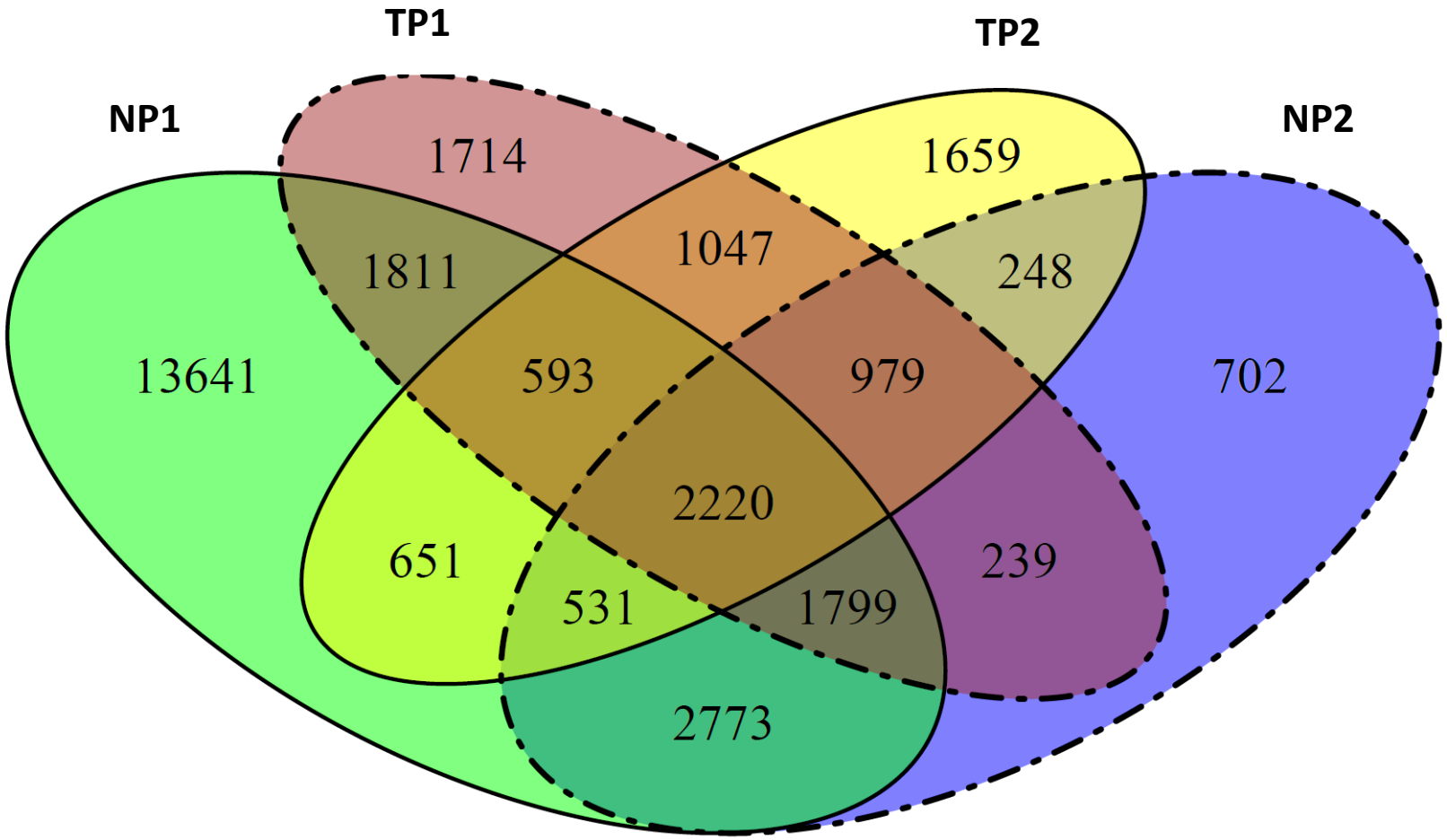

Figure 6

NPD	S	TPD	
-1.68	-369.20	-565.10	GRE(NR),IR3/A549-GR-ChIP-Seq(GSE32465)
-2.37	-330.90	-683.60	GRE(NR),IR3/RAW264.7-GRE-ChIP-Seq(Unpublished)/Homer
-3.28	-322.60	-554.70	PGR(NR)/EndoStromal-PGR-ChIP-Seq(GSE69539)
-0.41	-306.80	-569.60	ARE(NR)/LNCAP-AR-ChIP-Seq(GSE27824)
-45.93	-208.60	-180.30	Fra1(bZIP)/BT549-Fra1-ChIP-Seq(GSE46166)
-51.28	-203.90	-179.50	Fra2(bZIP)/Striatum-Fra2-ChIP-Seq(GSE43429)
-52.73	-195.80	-152.40	Fosl2(bZIP)/3T3L1-Fosl2-ChIP-Seq(GSE56872)
-36.02	-193.30	-175.90	JunB(bZIP)/DendriticCells-Junb-ChIP-Seq(GSE36099)
-42.22	-189.60	-172.40	Atf3(bZIP)/GBM-ATF3-ChIP-Seq(GSE33912)
-55.37	-188.90	-126.50	Jun-AP1(bZIP)/K562-cJun-ChIP-Seq(GSE31477)
-36.70	-178.20	-183.30	BATF(bZIP)/Th17-BATF-ChIP-Seq(GSE39756)
-28.22	-148.60	-161.40	AP-1(bZIP)/ThioMac-PU.1-ChIP-Seq(GSE21512)
-23.93	-107.50	-72.45	Bach2(bZIP)/OCILy7-Bach2-ChIP-Seq(GSE44420)
-3.41	-92.44	-17.81	WT1(Zf)/Kidney-WT1-ChIP-Seq(GSE90016)
-70.83	-64.44	-10.47	CRE(bZIP)/Promoter/Homer
-24.71	-63.78	-59.73	TEAD1(TEAD)/HepG2-TEAD1-ChIP-Seq(Encode)
-9.33	-61.79	-71.81	HOXB13(Homeobox)/ProstateTumor-HOXB13-ChIP-Seq(GSE56288)
-20.65	-60.64	-55.18	TEAD4(TEA)/Tropoblast-Tead4-ChIP-Seq(GSE37350)
-37.39	-54.81	-10.32	CArG(MADS)/PUER-Srf-ChIP-Seq(Sullivan_et_al.)
-7.90	-54.24	-17.16	Hoxc9(Homeobox)/Ainv15-Hoxc9-ChIP-Seq(GSE21812)
-12.91	-53.20	-56.94	TEAD(TEA)/Fibroblast-PU.1-ChIP-Seq(Unpublished)/Homer
-2.40	-52.92	-2.35	Zfp281(Zf)/ES-Zfp281-ChIP-Seq(GSE81042)
-10.35	-51.97	-35.37	TEAD2(TEA)/Py2T-Tead2-ChIP-Seq(GSE55709)
-14.79	-51.44	-30.48	NF-E2(bZIP)/K562-NFE2-ChIP-Seq(GSE31477)
-18.63	-47.97	-66.86	TEAD3(TEA)/HepG2-TEAD3-ChIP-Seq(Encode)
-8.28	-47.50	-37.69	Bach1(bZIP)/K562-Bach1-ChIP-Seq(GSE31477)
-11.33	-43.31	-20.12	Nrf2(bZIP)/Lymphoblast-Nrf2-ChIP-Seq(GSE37589)
-18.60	-42.21	-53.84	Stat3(Stat)/mES-Stat3-ChIP-Seq(GSE11431)
-63.98	-41.58	-30.04	JunD(bZIP)/K562-JunD-ChIP-Seq/Homer
-4.68	-41.21	-60.15	CDX4(Homeobox)/ZebrafishEmbryos-Cdx4.Myc-ChIP-Seq(GSE48254)
-9.32	-40.30	-49.68	Unknown(Homeobox)/Limb-p300-ChIP-Seq/Homer
-0.01	-40.29	-255.50	PR(NR)/T47D-PR-ChIP-Seq(GSE31130)
-4.14	-39.81	-5.71	Egr2(Zf)/Thymocytes-Egr2-ChIP-Seq(GSE34254)
-2.90	-39.22	-3.69	Egr1(Zf)/K562-Egr1-ChIP-Seq(GSE32465)
-11.28	-38.98	-47.99	Stat3+il21(Stat)/CD4-Stat3-ChIP-Seq(GSE19198)
-5.09	-38.54	-23.31	NF1(CTF)/LNCAP-NF1-ChIP-Seq(Unpublished)/Homer
-6.67	-34.33	-26.42	Hoxa11(Homeobox)/ChickenMSG-Hoxa11.Flag-ChIP-Seq(GSE86088)
-4.49	-34.09	-17.11	Hand2(bHLH)/Mesoderm-Hand2-ChIP-Seq(GSE61475)
-26.74	-33.88	-4.98	E-box(bHLH)/Promoter/Homer
-23.03	-32.46	-33.13	NFIL3(bZIP)/HepG2-NFIL3-ChIP-Seq(Encode)
-9.37	-31.14	-25.01	Hoxd11(Homeobox)/ChickenMSG-Hoxd11.Flag-ChIP-Seq(GSE86088)
-5.12	-30.13	-39.22	NFAT(RHD)/Jurkat-NFATC1-ChIP-Seq(Jolma_et_al.)
-40.81	-29.93	-7.81	RFX(HTH)/K562-RFX3-ChIP-Seq(SRA012198)
-83.39	-29.66	-0.75	NRF1(NRF)/MCF7-NRF1-ChIP-Seq(Unpublished)/Homer
-4.26	-29.28	-24.84	Hoxd10(Homeobox)/ChickenMSG-Hoxd10.Flag-ChIP-Seq(GSE86088)
-6.62	-28.95	-23.55	NFE2L2(bZIP)/HepG2-NFE2L2-ChIP-Seq(Encode)
-11.74	-28.63	-40.38	STAT4(Stat)/CD4-Stat4-ChIP-Seq(GSE22104)
-4.40	-28.07	-47.69	Hoxd13(Homeobox)/ChickenMSG-Hoxd13.Flag-ChIP-Seq(GSE86088)

NPD	S	TPD	
-10.09	-27.57	-15.14	FOXP1(Forkhead)/H9-FOXP1-ChIP-Seq(GSE31006)
-35.62	-27.16	-18.72	Atf2(bZIP)/3T3L1-Atf2-ChIP-Seq(GSE56872)
-37.39	-26.55	-9.30	Rfx1(HTH)/NPC-H3K4me1-ChIP-Seq(GSE16256)
-7.85	-26.54	-22.80	Foxo3(Forkhead)/U2OS-Foxo3-ChIP-Seq(E-MTAB-2701)
-0.06	-25.86	-50.67	Cdx2(Homeobox)/mES-Cdx2-ChIP-Seq(GSE14586)
-23.36	-25.83	-0.10	TFE3(bHLH)/MEF-TFE3-ChIP-Seq(GSE75757)
-1.96	-25.75	-21.33	Hoxa13(Homeobox)/ChickenMSG-Hoxa13.Flag-ChIP-Seq(GSE86088)
-9.13	-25.33	-24.72	STAT1(Stat)/HelaS3-STAT1-ChIP-Seq(GSE12782)
-42.60	-24.58	-0.38	E2F4(E2F)/K562-E2F4-ChIP-Seq(GSE31477)
-42.64	-22.73	-9.46	Rfx2(HTH)/LoVo-RFX2-ChIP-Seq(GSE49402)
-3.13	-21.27	-34.67	Bcl6(Zf)/Liver-Bcl6-ChIP-Seq(GSE31578)
-92.17	-19.75	0.00	YY1(Zf)/Promoter/Homer
-82.96	-19.69	-0.18	Sp1(Zf)/Promoter/Homer
-9.14	-18.52	-22.28	STAT5(Stat)/mCD4+-Stat5-ChIP-Seq(GSE12346)
-34.17	-18.42	-15.46	c-Jun-CRE(bZIP)/K562-cJun-ChIP-Seq(GSE31477)
-4.70	-18.32	-29.64	NFAT:AP1(RHD,bZIP)/Jurkat-NFATC1-ChIP-Seq(Jolma_et_al.)
-80.67	-17.49	-1.03	NRF(NRF)/Promoter/Homer
-153.30	-17.01	-1.60	Elk4(ETS)/Hela-Elk4-ChIP-Seq(GSE31477)
-137.80	-16.67	-0.23	Ronin(THAP)/ES-Thap11-ChIP-Seq(GSE51522)
-121.40	-16.43	-1.14	GFY-Staf(?,Zf)/Promoter/Homer
-169.80	-14.99	-1.17	Elk1(ETS)/Hela-Elk1-ChIP-Seq(GSE31477)
-47.46	-12.21	-1.54	CTCF(Zf)/CD4+-CTCF-ChIP-Seq(Barski_et_al.)
-133.60	-11.89	-0.18	ELF1(ETS)/Jurkat-ELF1-ChIP-Seq(SRA014231)
-166.40	-11.61	-0.15	ETS(ETS)/Promoter/Homer
-24.92	-11.51	-11.21	BMYB(HTH)/Hela-BMYB-ChIP-Seq(GSE27030)
-98.04	-9.30	-1.13	GFY(?)/Promoter/Homer
-4.55	-9.11	-24.08	NF1-halfsite(CTF)/LNCaP-NF1-ChIP-Seq(Unpublished)/Homer
-1.28	-8.51	-35.46	CEBP:AP1(bZIP)/ThioMac-CEBPb-ChIP-Seq(GSE21512)
-102.60	-8.43	-2.25	GABPA(ETS)/Jurkat-GABPa-ChIP-Seq(GSE17954)
-110.70	-7.23	-0.65	Fli1(ETS)/CD8-FLI-ChIP-Seq(GSE20898)
-76.30	-6.71	-4.72	ETS1(ETS)/Jurkat-ETS1-ChIP-Seq(GSE17954)
-1.63	-6.46	-19.27	HLF(bZIP)/HSC-HLF.Flag-ChIP-Seq(GSE69817)
-59.09	-5.41	-2.89	Etv2(ETS)/ES-ER71-ChIP-Seq(GSE59402)
-25.60	-4.54	-6.96	SPDEF(ETS)/VCaP-SPDEF-ChIP-Seq(SRA014231)
-62.80	-4.26	-0.75	EWS:FLI1-fusion(ETS)/SK_N_MC-EWS:FLI1-ChIP-Seq(SRA014231)
-25.89	-4.20	-7.22	MYB(HTH)/ERMYB-Myb-ChIPSeq(GSE22095)
-78.07	-3.77	-0.31	Elf4(ETS)/BMDM-Elf4-ChIP-Seq(GSE88699)
-75.01	-3.71	-3.26	ETV1(ETS)/GIST48-ETV1-ChIP-Seq(GSE22441)
-89.53	-3.32	-1.52	ETV4(ETS)/HepG2-ETV4-ChIP-Seq(ENCODE)
-44.95	-3.18	-5.71	ERG(ETS)/VCaP-ERG-ChIP-Seq(GSE14097)
-51.95	-3.13	-0.02	NFY(CCAAT)/Promoter/Homer
0.00	-2.31	-66.38	AR-halfsite(NR)/LNCaP-AR-ChIP-Seq(GSE27824)
0.00	-2.23	-28.34	CEBP(bZIP)/ThioMac-CEBPb-ChIP-Seq(GSE21512)
-41.44	-2.19	-0.64	EHF(ETS)/LoVo-EHF-ChIP-Seq(GSE49402)
-44.73	-1.24	-1.00	ELF5(ETS)/T47D-ELF5-ChIP-Seq(GSE30407)
-29.26	-0.63	-0.01	KLF3(Zf)/MEF-Klf3-ChIP-Seq(GSE44748)
-28.30	-0.51	-0.59	Sp5(Zf)/mES-Sp5.Flag-ChIP-Seq(GSE72989)

Figure 7

NPD	S	TPD	Canonical_Pathway
0.00	-5.42	0.00	Cell Cycle: G2/M DNA Damage Checkpoint Regulation
-0.39	-5.15	0.00	JAK/Stat Signaling
-0.89	-5.10	0.00	PI3K/AKT Signaling
0.00	-5.09	0.00	p53 Signaling
-1.81	-4.80	0.00	Insulin Receptor Signaling
0.00	-4.35	-0.34	ERK/MAPK Signaling
0.00	-4.19	-0.38	Acute Phase Response Signaling
-7.12	-4.04	0.00	Protein Ubiquitination Pathway
0.00	-3.97	0.00	CDK5 Signaling
-0.54	-3.93	0.00	14-3-3-mediated Signaling
0.00	-3.69	0.00	IL-9 Signaling
-0.80	-3.64	0.00	Molecular Mechanisms of Cancer
-3.40	-3.63	0.00	Regulation of eIF4 and p70S6K Signaling
0.00	-3.63	0.00	Breast Cancer Regulation by Stathmin1
0.00	-3.56	-1.15	GP6 Signaling Pathway
-0.29	-3.47	0.00	B Cell Receptor Signaling
0.00	-3.47	-1.52	HER-2 Signaling in Breast Cancer
-0.90	-3.42	0.00	IGF-1 Signaling
-1.84	-3.41	0.00	mTOR Signaling
-1.02	-3.35	-0.35	NRF2-mediated Oxidative Stress Response
0.00	-3.33	0.00	ILK Signaling
-1.06	-3.32	-0.61	Integrin Signaling
-0.32	-3.29	0.00	Actin Nucleation by ARP-WASP Complex
0.00	-3.25	0.00	Germ Cell-Sertoli Cell Junction Signaling
0.00	-3.22	0.00	Actin Cytoskeleton Signaling
-0.32	-3.21	-0.51	Signaling by Rho Family GTPases
-0.42	-3.15	-0.28	Regulation of Actin-based Motility by Rho
-7.59	-3.12	0.00	EIF2 Signaling
-1.07	-3.05	0.00	ATM Signaling
0.00	-3.05	0.00	Role of NFAT in Regulation of the Immune Response
0.00	-3.02	0.00	IL-7 Signaling Pathway
-0.76	-3.00	-0.51	Hereditary Breast Cancer Signaling
0.00	-2.98	-0.33	Chemokine Signaling
0.00	-2.96	0.00	Sertoli Cell-Sertoli Cell Junction Signaling
0.00	-2.88	-0.59	RhoA Signaling
-0.78	-2.81	-0.31	HIPPO signaling
-0.56	-2.80	0.00	PTEN Signaling
-0.52	-2.78	-0.30	IL-4 Signaling
0.00	-2.78	0.00	T Cell Receptor Signaling
0.00	-2.77	0.00	Protein Kinase A Signaling
-0.28	-2.72	-0.24	Virus Entry via Endocytic Pathways
0.00	-2.72	-0.33	Adrenomedullin signaling pathway
0.00	-2.72	0.00	Melanoma Signaling
0.00	-2.68	0.00	Ceramide Signaling
-0.32	-2.60	0.00	IL-15 Signaling
0.00	-2.60	0.00	RhoGDI Signaling
0.00	-2.55	0.00	Phospholipase C Signaling
-2.66	-2.53	-0.35	Hypoxia Signaling in the Cardiovascular System
-0.77	-2.53	-1.28	Glucocorticoid Receptor Signaling
0.00	-2.51	0.00	Docosahexaenoic Acid (DHA) Signaling
-1.68	-2.15	0.00	PDGF Signaling
-0.26	-2.12	-1.24	Paxillin Signaling
-1.12	-1.95	-1.40	ErbB Signaling
0.00	-1.95	-1.69	Caveolar-mediated Endocytosis Signaling
0.00	-1.92	-1.50	Coagulation System
-1.43	-1.69	0.00	Autophagy
-2.60	-1.66	-0.88	Aldosterone Signaling in Epithelial Cells
0.00	-1.61	-1.23	Glioma Signaling
0.00	-1.49	-3.03	Role of Macrophages, Fibroblasts and Endothelial Cells in Rheumatoid Arthritis
-2.12	-1.47	0.00	Superpathway of Inositol Phosphate Compounds
-3.37	-1.40	0.00	Sirtuin Signaling Pathway
-1.42	-1.39	0.00	Sonic Hedgehog Signaling
-0.78	-1.39	-1.36	UVA-Induced MAPK Signaling
-0.26	-1.30	-1.61	Agrin Interactions at Neuromuscular Junction
-1.09	-1.10	-1.31	Wnt/β-catenin Signaling
0.00	-1.07	-1.44	Th17 Activation Pathway

NPD	S	TPD	Canonical_Pathway
0.00	-1.03	-2.49	NF-κB Signaling
-1.44	-0.98	0.00	3-phosphoinositide Degradation
0.00	-0.97	-3.91	Hepatic Fibrosis / Hepatic Stellate Cell Activation
-1.42	-0.96	0.00	D-myo-inositol-5-phosphate Metabolism
-1.46	-0.91	0.00	Lysine Degradation II
-0.30	-0.91	-1.67	Non-Small Cell Lung Cancer Signaling
-1.18	-0.89	-1.71	RAR Activation
-0.32	-0.87	-1.78	IL-17A Signaling in Gastric Cells
0.00	-0.84	-3.04	UDP-N-acetyl-D-glucosamine Biosynthesis II
-1.64	-0.82	0.00	Mitochondrial Dysfunction
0.00	-0.73	-1.84	p38 MAPK Signaling
0.00	-0.65	-1.74	Phagosome Formation
-2.25	-0.64	0.00	Nucleotide Excision Repair Pathway
-1.55	-0.60	0.00	Purine Nucleotides De Novo Biosynthesis II
0.00	-0.58	-2.65	IL-10 Signaling
0.00	-0.58	-1.42	Inhibition of Matrix Metalloproteases
-1.44	-0.57	0.00	Glycogen Degradation II
-1.55	-0.57	-0.53	Huntington's Disease Signaling
-1.90	-0.56	-0.53	Estrogen Receptor Signaling
-0.30	-0.53	-1.36	MIF Regulation of Innate Immunity
0.00	-0.47	-2.15	Extrinsic Prothrombin Activation Pathway
-4.13	-0.31	-0.25	NER Pathway
-2.06	-0.27	0.00	Oxidative Phosphorylation
-2.48	-0.25	0.00	Fatty Acid β-oxidation I
-0.28	-0.23	-1.64	Toll-like Receptor Signaling
-2.33	-0.23	-0.62	DNA Methylation and Transcriptional Repression Signaling
0.00	-0.23	-1.53	MIF-mediated Glucocorticoid Regulation
-3.02	0.00	0.00	Arginine Degradation I (Arginase Pathway)
-3.01	0.00	0.00	Assembly of RNA Polymerase II Complex
-2.76	0.00	0.00	Telomere Extension by Telomerase
-2.37	0.00	-0.87	Valine Degradation I
-2.37	0.00	0.00	1D-myo-inositol Hexakisphosphate Biosynthesis II (Mammalian)
-2.15	0.00	0.00	Assembly of RNA Polymerase III Complex
-2.14	0.00	0.00	Aspartate Degradation II
-1.94	0.00	0.00	5-aminoimidazole Ribonucleotide Biosynthesis I
-1.94	0.00	0.00	D-glucuronate Degradation I
-1.81	0.00	0.00	TCA Cycle II (Eukaryotic)
-1.80	0.00	0.00	Heme Biosynthesis II
-1.71	0.00	0.00	D-myo-inositol (1,4,5)-trisphosphate Degradation
-1.66	0.00	0.00	Branched-chain α-keto acid Dehydrogenase Complex
-1.66	0.00	0.00	Heme Biosynthesis from Uroporphyrinogen-III I
-1.66	0.00	0.00	Glutathione Redox Reactions II
-1.66	0.00	0.00	Molybdenum Cofactor Biosynthesis
-1.66	0.00	0.00	Fatty Acid β-oxidation III (Unsaturated, Odd Number)
-1.63	0.00	0.00	D-myo-inositol (1,3,4)-trisphosphate Biosynthesis
-1.61	0.00	0.00	Role of Wnt/GSK-3β Signaling in the Pathogenesis of Influenza
-1.46	0.00	0.00	2-ketoglutarate Dehydrogenase Complex
-1.46	0.00	0.00	Tetrahydrofolate Salvage from 5,10-methenyltetrahydrofolate
-1.46	0.00	0.00	Lysine Degradation V
-1.46	0.00	0.00	2-oxobutanoate Degradation I
-1.44	0.00	0.00	Cleavage and Polyadenylation of Pre-mRNA
-1.36	0.00	0.00	Activation of IRF by Cytosolic Pattern Recognition Receptors
-0.97	0.00	-2.66	Leucine Degradation I
-0.75	0.00	-1.63	Proline Degradation
0.00	0.00	-1.97	Inflammasome pathway
0.00	0.00	-1.90	Phospholipases
0.00	0.00	-1.82	Pyridoxal 5'-phosphate Salvage Pathway
0.00	0.00	-1.80	Asparagine Degradation I
0.00	0.00	-1.80	LXR/RXR Activation
0.00	0.00	-1.66	TREM1 Signaling
0.00	0.00	-1.50	Heme Degradation
0.00	0.00	-1.50	Sperm Motility
0.00	0.00	-1.46	Altered T Cell and B Cell Signaling in Rheumatoid Arthritis
0.00	0.00	-1.39	Communication between Innate and Adaptive Immune Cells
0.00	0.00	-1.37	Salvage Pathways of Pyrimidine Ribonucleotides
0.00	0.00	-1.33	Ceramide Biosynthesis

Table 1

Group	**NP**	**TP**
Sample size	3	3
Number of Gene Expressed	14899	15260
Expressed in Both Groups	95.7 %	93.4 %

Table 2

Gene Ontology Term	*p*
Enriched at the NP stage	
Transcription	3.18×10^{-15}
RNA-binding	7.60×10^{-3}
Histone deacetylase activity	3.84×10^{-3}
Enriched at the TP stage	
Innate immunity	1.62×10^{-20}
Protease	7.32×10^{-7}
Carbohydrate transport and metabolism	1.62×10^{-3}

Table 3

Change of Molecular activities	Human Activation z-score	Human Enrichment *p* value	Mouse Activation z-score	Mouse Enrichment *p* value
TGFβ	2.40	1.05×10^{-15}	4.38	2.13×10^{-13}
PDGF-BB	2.82	1.67×10^{-18}	3.49	9.03×10^{-17}
PI3K	5.04	2.38×10^{-14}	2.57	4.16×10^{-10}
TNF	8.31	2.92×10^{-73}	2.36	6.75×10^{-43}
AP-1	2.41	3.66×10^{-12}	2.16	8.12×10^{-5}
ERK	3.87	3.44×10^{-12}	3.11	3.85×10^{-8}
p53	2.39	5.00×10^{-53}	3.03	4.02×10^{-54}
STAT3	2.87	5.04×10^{-27}	1.95	1.97×10^{-6}
D-Glucose	2.39	2.44×10^{-20}	2.63	9.84×10^{-18}

Table 4

Class	Number of Total Enriched Motifs	List of Uniquely Enriched Motifs
I	128	AMYB, Arnt:Ahr, Ascl1, Atoh1, BMYB, c-Myc, E2F1, E2F6, Egr1, Eomes, ERE, Esrrb, Fox:Ebox, FOXA1, FXR, Gfi1b, HNF4a, HOXA2, KLF5, Lhx2, Lhx3, Max, MITF, MYB, MyoD, Nanog, NeuroD1, Nkx6.1, PAX5, Pax8, Pdx1, PPARE, PGR, PRDM1, PRDM9, PU.1-IRF, Rbpj1, RUNX1, RUNX2, RXR, Smad2, SPDEF, TATA-Box, THRa, VDR
II	82	GFX, GFY, ZBTB33
III	121	CEBP, EKLF, Hnf1, HRE, Mef2a, NF1, Nr5a2, Nur77, PAX3, RORgt, RUNX, Tbx20, Usf2

Table 5

	Positively Correlated	Negatively Correlated
Number of dynamic OCRs in association with DEGs	2989	1660
Number of DEGs in association with dynamic OCRs	1461	980

Table 6

Canonical Pathways	-Log(*p*)	Category
Signaling by Rho Family GTPases	2.80	Positively Correlated DEGs-OCRs
Actin Cytoskeleton Signaling	2.00	Positively Correlated DEGs-OCRs
NFκB Signaling	1.60	Positively Correlated DEGs-OCRs
Gap Junction Signaling	1.66	Positively Correlated DEGs-OCRs
Glycolysis	1.63	Positively Correlated DEGs-OCRs
Adrenomedullin signaling pathway	2.42	Negatively Correlated DEGs-OCRs
eNOS Signaling	2.06	Negatively Correlated DEGs-OCRs
Relaxin Signaling	1.79	Negatively Correlated DEGs-OCRs
PDGF Signaling	1.98	Negatively Correlated DEGs-OCRs
HIPPO signaling	1.68	Negatively Correlated DEGs-OCRs

Table 7. Genome-wide PGR occupying sites relative to gene bodies

	NP1	NP2	TP1	TP2	Background
Promoter	23.6 %	25.4 %	19.3 %	9.6 %	2.4 %
5’ UTR	10.7 %	10.0 %	7.1 %	2.4 %	0.4 %
Coding Exon	4.2 %	2.8 %	2.1 %	0.8 %	1.9 %
Intron	33.5 %	31.6 %	36.2 %	41.5 %	41.6 %
3’ UTR	1.4 %	1.5 %	1.3 %	1.2 %	1.4 %
Downstream of gene body	3 %	2.2 %	2.3 %	2.4 %	2.2 %
Distal intergenic region	23.4 %	26.5 %	31.8 %	42.0 %	50 %

Table 8

Motif		Enrichment *p* value (log_{10})	
		NP	TP
	PGR	-40.44	-803.7
	STAT	-36.08	-136.3
	CArG	-63.84	-87.38
	MyoD	-43.74	-21.85
	SMAD2	-32.38	-37.57

Table 9

NP Distinct	Shared by NP and TP	TP Distinct
PGR occupying intervals examined		
2773	2220	1047
Number of PGR occupying intervals in association with active genes in the myometrium		
2252	1510	593
Number of myometrial active genes in association with PGR occupying intervals		
1431	589	183

Table 10

Gene	Region of Interest	Binding Events Detected Per 1000 Cells			
		NP3	NP4	TP3	TP4
ENO1	chr1:8938001-8939564	25.93 ± 1.89	12.46 ± 1.44	0.91 ± 0.38	0.71 ± 0.93
LDHA	chr11:18415880-18416428	30.15 ± 3.49	11.42 ± 1.45	1.56 ± 0.42	2.35 ± 0.68
PLCL1	chr2:199107091-199107777	119.13 ± 8.45	7.77 ± 1.76	9.44 ± 0.31	6.40 ± 0.79
Untr12	Chromosome 12	0.15 ± 0.15	0.00 ± 0.00	0.13 ± 0.23	0.00 ± 0.00

Figure S1

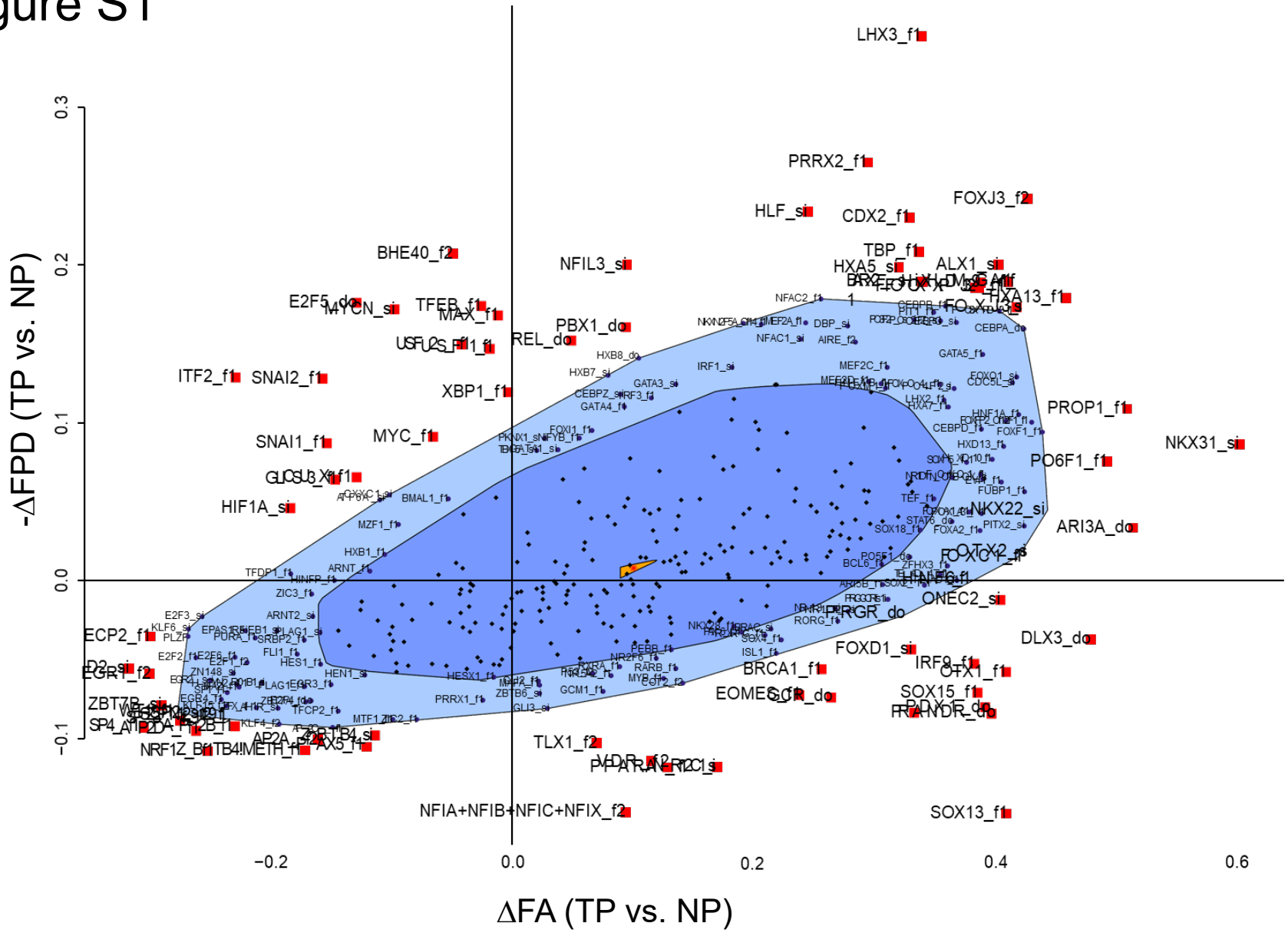
-ΔFPD (TP vs. NP)
ΔFA (TP vs. NP)
0.3
0.2
0.1
0.0
−0.1
−0.2
0.0
0.2
0.4
0.6
LHX3_f1
PRRX2_f1
FOXJ3_f2
HLF_si
CDX2_f1
TBP_f1
HXA5_si
ALX1_si
HXA13_f1
BHE40_f2
NFIL3_si
E2F5_do
MYCN_si
TFEB_f1
MAX_f1
PBX1_do
REL_do
USF2S_f1
ITF2_f1
SNAI2_f1
XBP1_f1
PROP1_f1
SNAI1_f1
MYC_f1
NKX31_si
PO6F1_f1
HIF1A_si
NKX22_si
ARI3A_do
ONEC2_si
ECP2_f1
DLX3_do
FOXD1_si
BRCA1_f1
IRF9_f1
OTX1_f1
SOX15_f1
TLX1_f2
NFIA+NFIB+NFIC+NFIX_f2
SOX13_f1